

End-to-end Learning of Sparse Interventions on Activations to Steer Generation

Pau Rodríguez*¹ Michal Klein¹ Eleonora Gualdoni¹ Arno Blaas¹
Luca Zappella¹ Marco Cuturi¹ Xavier Suau*¹

Abstract

The growing use of generative models in daily life calls for efficient mechanisms to control their generation, to *e.g.*, produce safe content or provide users with tools to explore style changes. Ideally, such mechanisms should be cheap, both at train and inference time, while preserving output quality. Recent research has shown that such mechanisms can be obtained by intervening exclusively on model *activations*, with the goal of correcting *distributional* differences between activations seen when using prompts from a source vs. a target set (*e.g.*, toxic and non-toxic sentences). While cheap, these fast methods are inherently crude: their maps are tuned locally, not accounting for their impact on downstream layers, resulting in interventions that cause unintended shifts when used out-of-sample. We propose in this work linear end-to-end activation steering (LinEAS), an approach trained with a global loss that accounts simultaneously for all layerwise distributional shifts. In addition to being more robust, the loss used to train LinEAS can be regularized with sparsifying norms, which can automatically carry out neuron and layer selection. Empirically, LinEAS only requires a handful of samples to be effective, and beats similar baselines on toxicity mitigation, while performing on par with far more involved finetuning approaches. We show that LinEAS interventions can be *composed*, study the impact of sparsity on their performance, and showcase applications in text-to-image diffusions.

1. Introduction

Generative models are typically trained in two distinct phases. The first phase, known as pre-training, involves learning from a large corpus of data using tasks like next-

*Equal contribution ¹Apple. Correspondence to: Pau Rodríguez <pau.rodriguez@apple.com>.

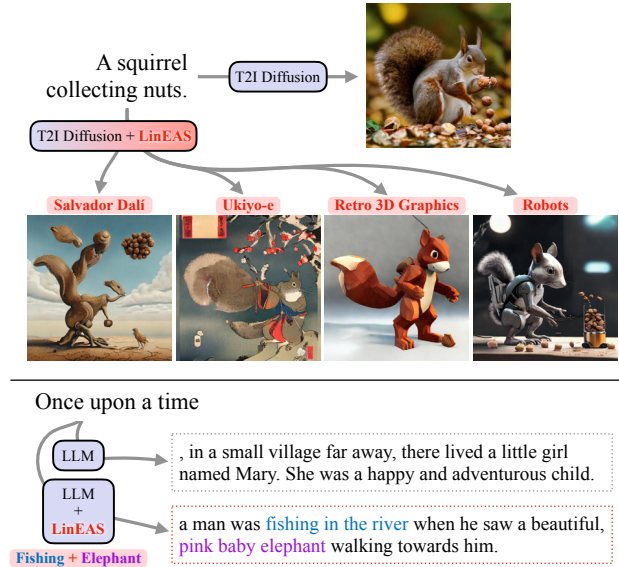


Figure 1. LinEAS learns lightweight maps to steer pretrained model activations. With LinEAS, we can induce very precise styles in text-to-image diffusion (top), and even compose maps to induce concepts simultaneously in LLMs (bottom).

token prediction or text-to-image generation. This is followed by a fine-tuning phase designed to align the model towards a more specific, desired behavior. This alignment can be achieved through instruction fine-tuning (Wei et al., 2022), reinforcement learning from human feedback (RLHF) (Ouyang et al., 2022) for LLMs, or guidance (Ho & Salimans, 2022) and LoRA adapters (Luo et al., 2024) in text-to-image diffusion. Many of these approaches propose to modify the model’s internal mechanisms, realigning its parameters by leveraging new data with, ideally, a minimal impact on the utility of the model.

Finetuning on a budget. The rapid growth of model sizes, coupled with the potentially infinite combination of steering goals that users may need, call for steering mechanisms that are data-efficient (require few annotated samples) cheap to train (potentially on device), memory-efficient (small set of parameters), and incur little to no overhead on inference time compute. We frame our paper in this context, observing that this opportunity has created a need for approaches that advocate a better understanding of features (Geiger et al.,

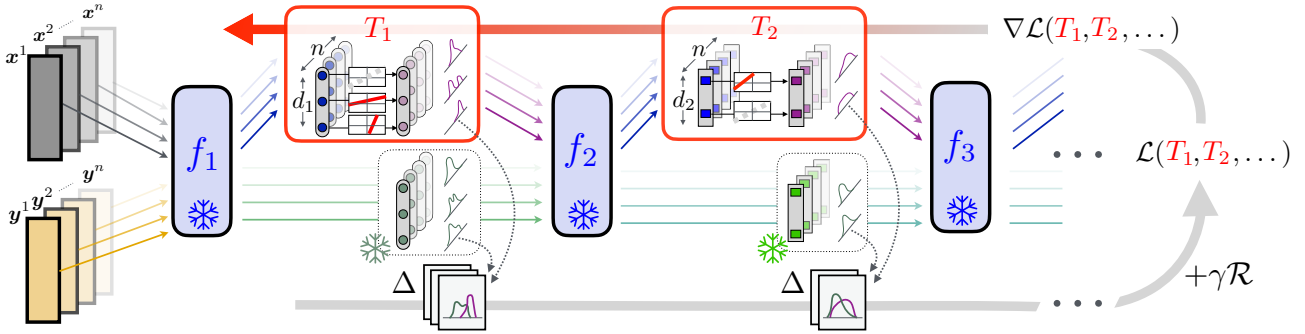


Figure 2. Given a frozen computational graph (blue) of $L + 1$ layers of interest, we interlace it with L transport blocks (red). Each transport is defined as a collection of *coordinate-wise* affine transformations, as displayed in the 3 and 2 boxes for maps T_1 and T_2 respectively. All transport maps are jointly trained to minimize a sum of distributional losses Δ collected between the neural activation distributions collected from samples $\mathbf{x}_1, \dots, \mathbf{x}_n \sim p$ (one shade of grey per sample) and $\mathbf{y}_1, \dots, \mathbf{y}_n \sim q$ (resp. yellow). That loss is penalized by a regularization term \mathcal{R} . We learn the parameters of these maps *jointly* by minimizing the penalized sum of Δ terms, where Δ is a 1D Wasserstein distances evaluated on the d_ℓ activations of layer ℓ . Using a global optimization, we can consider sparsifying regularizers, to, e.g., carry out a sparse selection of a subset of activations that require interventions. For instance, when adding a regularizer that promotes sparsity, both T_1 and T_2 do not intervene on a neuron, the first and the second, respectively.

2024) that can help control specific behaviors or properties (Suau et al., 2022; Rimsky et al., 2023; Zou et al., 2023; Li et al., 2024; Rodriguez et al., 2025; Yin et al., 2024a). As these modifications are usually characterized by a small number of parameters, they can be estimated with just a few hundred sentences (Suau et al., 2024; Turner et al., 2023). For example, Rimsky et al. (2023); Li et al. (2024) shift the activations by applying a constant vector derived from desired and undesired data sets (e.g., non-toxic and toxic); or Suau et al. (2024) mitigate toxicity by adjusting activations to neuron expertise. Current methods are successful but do not preserve the activation distribution present during the model’s training. Because generative models are known to be sensitive to shifts in distributions (Huu-Tien et al., 2024; Sclar et al., 2024), even minor modifications such as translations can move activations out-of-distribution, potentially hindering both the conditioning and output quality.

Our contributions. We propose a novel framework to steer activations, using simple maps trained jointly across layers:

- We propose a global loss to train interleaved transportation maps, linear end-to-end activation steering (LinEAS), using a global loss that tracks the impact of any map on the distribution of its subsequent layers in the computational graph (e.g., T_1 on distribution shifts handled by T_2 in Fig. 2). Similar to (Rodriguez et al., 2025), we restrict our search to coordinate-wise affine maps. Unlike their work, our loss is not local, but global, enforcing a global distributional alignment across all layers (see Fig. 2).
- We leverage our global optimization approach to introduce *sparse group lasso* regularizers (Simon et al., 2013) that can detect a small subset of activations that matter to achieve the desired transfer.

- We confirm in our experiments that global optimization and sparse regularizers yield, when combined, results that improve significantly on baselines to reduce toxicity; For instance, we improve on (Li et al., 2024; Rodriguez et al., 2025) using 100 or 1000 times less intervened neurons.
- We study how *two* sparse LinEAS interventions trained independently can be combined sequentially, and validate that they exhibit the desired property of inducing simultaneously two concepts at generation, hence cementing the potential of LinEAS to provide a data-efficient approach to combine multiple concepts (see Figure 1).
- We show how LinEAS can be used to steer style in text-to-image diffusion generation, providing visually appealing results and quantitative improvements over baselines.

2. Related Work

The growing capabilities and prevalence of LLMs (Brown et al., 2020), along with the rising costs of fine-tuning and alignment, have driven research into their controllability through cheaper forms of interventions. Most relevant to our work are activation steering methods, also called representation engineering (Zou et al., 2023). These methods learn lightweight interventions on a subset of activations of generative models, to steer them towards a desired property.

Single-property steering. Most works focus on controlling a single property through activation steering (e.g., toxicity). The earliest among those methods, ACTADD (Turner et al., 2023), uses a contrast prompt (one positive and one negative example) to construct a shift vector that is added to activations for steering during inference. CAA (Rimsky et al., 2023) extends ACTADD by calculating the shift vector for

steering based on a dataset of contrast pairs (rather than a single pair), adding the mean difference during inference time for steering. ITI-C (Li et al., 2024) uses a shift vector orthogonal to the hyperplane learned by a binary linear classifier on the activations from two sets of sentences. With a different approach, AURA by Suau et al. (2024) dampens activations proportionally to each neuron’s ability to classify toxic and non-toxic sentences, effectively mitigating toxicity. REPE by Zou et al. (2023) proposes to compute steering vectors at inference time based on prompt pairs. Wu et al. (2024) considers activations relationships using a low-rank projection to exchange information with a counterfactual representation and Geiger et al. (2024) consider interventions on rotations of subsets of features. Closest to our work, Lin-ACT (Rodriguez et al., 2025) uses an affine map to steer activations.

Multi-property steering. Few works tackle the problem of simultaneously steering towards multiple properties of model generations. van der Weij et al. (2024) control multiple properties by building on the mean shift vector approach (CAA; Rimsky et al., 2023), reporting limited success when trying to simultaneously control properties such as anti-immigration, agreeableness, myopia, sycophancy, and wealth seeking. Liu et al. (2023) qualitatively demonstrate that their proposed method can simultaneously control up to three properties out of safety, politeness, positive sentiment, formality, and being emotive. Scalena et al. (2024) propose an approach that can simultaneously control safety, formality, and language of generations (e.g., Italian). Zhang et al. (2025) simultaneously steer activations to control sentiment, formality, and topic (sports) of model generations.

3. End-to-end Learning of Steering Maps

We propose LinEAS, a method to optimize activation-specific interventions in a joint manner. Our hypothesis is that a global estimation that exploits causal interdependencies between activations across layers is needed to maintain the model’s utility while achieving the steering goal.

3.1. Interventions Setup and Distributional Loss

We consider a generative model and target a set of L intermediate activation layers. We describe the model as a composition of $L + 1$ abstract pretrained functions, where the output, given an input prompt $x \in \mathcal{S}$, can be written as

$$o = f_{L+1} \circ f_L \circ \dots \circ f_1(x).$$

For convenience, we denote d_ℓ the dimension of the activations obtained at layer ℓ , i.e., the size of the activation vector $f_\ell \circ \dots \circ f_1(x)$. We interlace this pretrained computational graph of $L + 1$ intermediate frozen layers with L

comparatively much simpler vector-to-vector maps:

$$o = f_{L+1} \circ T_L \circ f_L \circ \dots \circ T_2 \circ f_2 \circ T_1 \circ f_1(x).$$

where for $1 \leq \ell \leq L$, the map $T_\ell : \mathbb{R}^{d_\ell} \rightarrow \mathbb{R}^{d_\ell}$ acts on the intermediate activations observed after layer ℓ , by altering its coordinates and outputting a vector of the same size.

Layerwise Distributional Losses. We consider two distinct probability distributions of prompts, the source p and the desired target q , both in $\mathcal{P}(\mathcal{S})$. We view each prompt realization through the lens of their sequence of L activations. In practice, this means having access to samples $x^1, \dots, x^n \sim p$ and $y^1, \dots, y^n \sim q$, tracking their execution trace of their $\ell \leq L + 1$ activations, either modified through interleaved transports for samples from p

$$\xi_\ell^i := T_\ell \circ f_\ell \circ T_{\ell-1} \circ \dots \circ T_1 \circ f_1(x^i), \quad \ell \leq L, \quad (1)$$

or ran through the original network for samples of q :

$$\eta_\ell^j := f_\ell \circ \dots \circ f_1(y^j), \quad \ell \leq L. \quad (2)$$

Our goal is to learn *jointly* all L transport maps so that, for each $\ell \leq L$, the families of vectors $(\xi_\ell^i)_i$ and $(\eta_\ell^j)_j$ are *similar* with respect to a distributional metric Δ between probability measures, making the cost below small:

$$\mathcal{C}(T_1, \dots, T_L; (x^i)_i, (y^j)_j) = \sum_{\ell \leq L} \Delta((\xi_\ell^i)_i, (\eta_\ell^j)_j). \quad (3)$$

Differences with ITI-C and Lin-ACT. The fundamental difference between our approach and that explored in previous steering works (Li et al., 2024; Rodriguez et al., 2025) is that their optimization problem is *split* across layers: each T_ℓ is trained *independently*, using closed forms, to minimize one single distributional difference $\Delta((\xi_\ell^i)_i, (\eta_\ell^j)_j)$, assuming all other layers are frozen. While arguably much faster, this also generates causal inconsistencies, which can be partially resolved as in (Rodriguez et al., 2025) by using a sequential approach: when $T_{\ell-1}$ is trained, $T_{\ell-1}$ is reused to recompute all activation distributions used for T_ℓ . We claim that this suboptimality is to blame for poor generalization. This independent approach also precludes trade-offs when choosing which activations to turn on/off across layers, which we can easily explore using sparsity regularizers.

Sliced Wasserstein Losses. To define Δ at each layer, we adopt the approach of Rodriguez et al. (2025) and use d univariate Wasserstein distances between the d marginal distributions. The activations can be arranged as matrices $U := [\xi_\ell^1, \dots, \xi_\ell^n]$ and $V = [\eta_\ell^1, \dots, \eta_\ell^n]$, both in $\mathbb{R}^{n \times d_\ell}$. To compute their 1D-Wasserstein distance (Santambrogio, 2015, Chap. 2), these activations must be first sorted in increasing order along the feature axis:

$$\tilde{U} = \text{sort}(U, \text{axis} = -1), \tilde{V} = \text{sort}(V, \text{axis} = -1)$$

to define the sliced Wasserstein distance (Rabin et al., 2012) computed exclusively on the *canonical directions*, namely:

$$\Delta(U, V) := \sum_{j=1}^d W_2^2(U_{\cdot j}, V_{\cdot j}) = \frac{1}{n} \sum_{j=1}^d \|\tilde{U}_{\cdot j} - \tilde{V}_{\cdot j}\|^2. \quad (4)$$

3.2. Parameterization and Regularization

Building on the approach outlined by Rodriguez et al. (2025), we propose to parameterize each map T_ℓ as an affine map for each activation $\ell \leq L$, namely for $z \in \mathbb{R}^{d_\ell}$, one has

$$T_\ell(z) := \omega_\ell \odot z + b_\ell, \quad \omega_\ell, b_\ell \in \mathbb{R}^{d_\ell}, \quad (5)$$

where \odot is the element-wise product. We write $\mathbf{w} := (\omega_1, \dots, \omega_L)$ and $\mathbf{b} := (b_1, \dots, b_L)$ for the collections of all scale and intercept parameters. In what follows since each map T_ℓ is entirely parameterized through its scale/intercept parameters \mathbf{w}, \mathbf{b} , we overload notations to define

$$\mathcal{C}(\mathbf{w}, \mathbf{b}; (\mathbf{x}^i)_i, (\mathbf{y}^j)_j) := \mathcal{C}(T_1, \dots, T_{L-1}; (\mathbf{x}^i)_i, (\mathbf{y}^j)_j).$$

Sparse Group Regularization. We propose to use a sparsity regularizer that will carry out both *layer* and *within-layer* selection of activations. This can be achieved by using structured regularization, using either 1-norms or 2-norms,

$$\begin{aligned} \mathcal{R}_1(\mathbf{w}, \mathbf{b}) &:= \sum_{\ell} \|\omega_\ell - \mathbf{1}\|_1 + \|b_\ell\|_1. \\ \mathcal{R}_G(\mathbf{w}, \mathbf{b}) &:= \sum_{\ell} \sqrt{d_\ell} (\|\omega_\ell - \mathbf{1}\|_2 + \|b_\ell\|_2). \end{aligned}$$

resulting in a *sparse group lasso* regularizer (Simon et al., 2013; Yoon & Hwang, 2017), $\mathcal{R} := \lambda_1 \mathcal{R}_1 + \lambda_G \mathcal{R}_G$, which can be added to the cost to result in:

$$\mathcal{L}(\mathbf{w}, \mathbf{b}) := \mathbb{E}_{\substack{(\mathbf{x}^i)_i \sim p, \\ (\mathbf{y}^j)_j \sim q}} [\mathcal{C}(\mathbf{w}, \mathbf{b}; (\mathbf{x}^i)_i, (\mathbf{y}^j)_j)] + \gamma \mathcal{R}(\mathbf{w}, \mathbf{b}), \quad (6)$$

where γ controls the amount of sparsity, *i.e.*, larger γ will result in fewer activations and/or layers being intervened on, with solution such that $\omega \approx \mathbf{1}$ and $b \approx \mathbf{0}$. Recall that for a vector $z \in \mathbb{R}^d$, the proximal operators of the 1-norm (a.k.a. soft-thresholding) and 2-norm are given by:

$$\begin{aligned} \text{ST}_\tau(z) &:= \text{sign}(z) \odot \max(|z| - \tau, \mathbf{0}), \\ \text{Prox}_{\tau, \|\cdot\|_2}(z) &:= \left(1 - \frac{\lambda_1}{\|z\|_2}\right)_+ z. \end{aligned} \quad (7)$$

3.3. Optimization

Proximal SGD. We optimize \mathcal{L} in (6) with proximal stochastic gradient descent (PSGD) with a learning rate of 0.1 and cosine decay. We assume access to 2 sets of N prompts

Algorithm 1 Proximal E2E Training Step.

- 1: **Require:** prompts $(\mathbf{x}^i)_i \sim p, (\mathbf{y}^j)_j \sim q$, LR ρ .
 - 2: (pre-) compute activations $\boldsymbol{\eta}_\ell^i, i \leq n, \ell \leq L$ \triangleright Eq.(3)
 - 3: compute activations lists $\boldsymbol{\xi}_\ell^i, i \leq n, \ell \leq L$. \triangleright Eq.(1)
 - 4: set loss to $\mathcal{C} = 0$
 - 5: **for** $\ell \leq L$ **do** \triangleright Forward
 - 6: $Z := [\boldsymbol{\xi}_\ell^1, \dots, \boldsymbol{\xi}_\ell^n] \text{diag}(\omega_\ell) + \mathbf{1}_n b_\ell^T \in \mathbb{R}^{n \times d_\ell}$
 - 7: $V := [\boldsymbol{\eta}_\ell^1, \dots, \boldsymbol{\eta}_\ell^n] \in \mathbb{R}^{n \times d_\ell}$
 - 8: $\mathcal{C} \leftarrow \mathcal{C} + \Delta(Z, V)$ \triangleright ℓ -layer loss, Eq. (4)
 - 9: **end for**
 - 10: **for** $\ell \leq L$ **do**
 - 11: $g_\omega, g_b \leftarrow \nabla_{\omega_\ell, b_\ell} \mathcal{C}$ \triangleright Backpropagation
 - 12: $\omega_\ell, b_\ell \leftarrow \omega_\ell - \rho g_\omega, b_\ell - \rho g_b$ \triangleright Updates
 - 13: $\omega_\ell \leftarrow \text{Prox}_{\gamma \lambda_G \|\cdot\|_2} \circ \text{ST}_{\gamma \lambda_1}(\omega_\ell - \mathbf{1}) + \mathbf{1}$ \triangleright Eq. (7)
 - 14: $b_\ell \leftarrow \text{Prox}_{\gamma \lambda_G \|\cdot\|_2} \circ \text{ST}_{\gamma \lambda_1}(b_\ell)$ \triangleright Eq. (7)
 - 15: **end for**
-

$(\mathbf{x}^i)_{i=1}^N$ and $(\mathbf{y}^j)_{j=1}^N$ and run PSGD on minibatches of size n , *i.e.*, batches of activations $(\boldsymbol{\xi}_\ell^i)_i$ and $(\boldsymbol{\eta}_\ell^i)_i$ of size n . Note that activations originating from \mathbf{y}^i use the untouched network, and can be pre-computed beforehand. See Algo. 1 for the description of a single optimization step.

Sparsity and Refitting. When $\gamma \gg 0$, several coordinates of ω_ℓ and b_ℓ (parameters of T_ℓ) will collapse to 1 or 0, respectively. While this is desired, non-zero parameters typically suffer from shrinking, where the regularization terms $\mathcal{R}_1, \mathcal{R}_G$ dampen the effect of \mathcal{C} . A typical solution to this phenomenon is to perform m_{post} training steps updating only those non-collapsed parameters, a practice known as refitting in regression (Belloni & Chernozhukov, 2013; Chzen et al., 2019). We have not observed improvements when refitting parameters, and therefore do not use it. We observe that the entries of $\omega_\ell - \mathbf{1}$ and b_ℓ have similar scales (see Fig. 8) and choose to use the same regularization strength.

4. Experimental Results

4.1. Toxicity Mitigation in LLMs

We compare the effectiveness of LinEAS at toxicity mitigation with ITI-C (Li et al., 2024) and Lin-ACT (Rodriguez et al., 2025) on four LLMs, by aligning the activations of $N = 32$ toxic to 32 non-toxic sentences sampled from the Jigsaw dataset (Adams et al., 2017).

Toxicity Metrics. We evaluate toxicity mitigation on the *RealToxicityPrompts* (RTP) dataset (Gehman et al., 2020) and the *Thoroughly Engineered Toxicity* (TET) dataset (Luong et al., 2024). For RTP, we follow Rodriguez et al. (2025) and sample 1000 prompts from the dataset and let the model (intervened or not) complete them. For TET, we use the 2546 prompts provided. Then, we score the generations using the open-source Roberta toxicity classifier (RTC) (Logacheva

Model	Method	#Params	Tox _{RTP} ^{RTP} (↓)	Tox _{RTP} ^{TET} (↓)	PPL _{WIK} (↓)	MMLU (↑)
Q1.5B	None	-	3.00 _{0.54}	23.09 _{0.67}	13.67 _{0.00}	60.95 _{0.00}
	LRTC-RL	0.54M	1.07 _{0.40}	7.94 _{0.01}	13.70 _{0.10}	60.78 _{0.17}
	ITI-C	0.043M	1.87 _{0.21}	18.16 _{0.62}	12.39 _{0.09}	60.88 _{0.08}
	Lin-Act	0.086M	1.50 _{0.35}	13.88 _{1.72}	13.88 _{0.16}	60.09 _{0.25}
	LinEAS	0.086M	1.07 _{0.46}	12.70 _{0.74}	14.10 _{0.07}	59.97 _{0.16}
G2-2B	None	-	4.00 _{0.45}	13.39 _{1.42}	14.79 _{0.00}	53.03 _{0.00}
	LRTC-RL	0.8M	0.83 _{0.25}	3.47 _{0.01}	15.38 _{0.17}	52.56 _{0.11}
	ITI-C	0.06M	1.17 _{0.60}	7.15 _{0.92}	14.00 _{0.11}	52.78 _{0.23}
	Lin-Act	0.12M	1.60 _{0.32}	7.76 _{0.39}	14.78 _{0.12}	52.43 _{0.57}
	LinEAS	0.24M	0.73 _{0.10}	4.02 _{0.68}	15.46 _{0.21}	52.22 _{0.40}
D7B	None	-	4.30 _{0.70}	18.62 _{0.51}	8.49 _{0.00}	48.31 _{0.00}
	LRTC-RL	1.97M	1.97 _{0.38}	5.07 _{0.00}	8.67 _{0.05}	47.76 _{0.34}
	ITI-C	0.13M	2.83 _{0.40}	15.18 _{2.00}	7.71 _{0.07}	48.47 _{0.25}
	Lin-Act	0.25M	2.23 _{0.69}	11.08 _{0.76}	8.67 _{0.03}	47.71 _{0.27}
	LinEAS	0.25M	2.30 _{0.14}	12.09 _{0.83}	8.38 _{0.05}	48.13 _{0.07}
Q7B	None	-	3.92 _{0.59}	25.16 _{0.92}	10.67 _{0.00}	74.26 _{0.00}
	LRTC-RL	1.26M	1.30 _{0.44}	6.59 _{0.01}	10.68 _{0.06}	74.08 _{0.15}
	ITI-C	0.10M	2.97 _{0.21}	20.68 _{2.21}	9.56 _{0.02}	74.20 _{0.07}
	Lin-Act	0.20M	2.25 _{0.13}	16.04 _{0.95}	10.77 _{0.09}	73.56 _{0.08}
	LinEAS	0.20M	1.88 _{0.19}	15.39 _{0.60}	10.83 _{0.25}	73.56 _{0.07}

Table 1. Toxicity mitigation on the RTP and TET datasets using four different models, Q1.5B: Qwen-1.5B, G2-2B: Gemma2-2B, D7B: DeepSeek-7B and Q7B: Qwen-7B. We report results at low ($N = 32$ sentences to estimate the interventions) data regime. For each method, we use the best intervention layers according to an ablation study. See Table 2 in Appendix for an ablation with larger training size. Results for LinEAS improve significantly on ITI-C and Lin-Act with similar impact on quality metrics. The quality of these interventions is often on par with the strong baseline LRTC-RL, despite this approach being far more involved (both in terms of parameter size, access to ground truth labelling oracle RTC, and compute).

et al., 2022). We report $\text{Tox}_{\text{RTC}}^{\text{RTP}}$ and $\text{Tox}_{\text{RTC}}^{\text{TET}}$, the respective percentage of generations flagged as toxic on RTP and TET.

Utility metrics. To measure whether the utility of the model is affected by these interventions, we report PPL_{WIK} , the perplexity obtained on a fixed set of 20k Wikipedia sentences (Wikimedia), as well as the overall 5-shot accuracy on the MMLU compendium (Hendrycks et al., 2021).

Strong Baseline: LRTC-RL. In addition to ITI-C and Lin-Act, both natural competitors to LinEAS, we introduce a much stronger baseline that assumes an oracle knowledge of RTC, the classifier used to compute *test-time metrics*. To propose such a strong contender, we borrow inspiration from RLHF (Ouyang et al., 2022) and train a LoRA adapter using the *ground-truth* labelling oracle RTC, giving it a significant advantage. Following Ouyang et al. (2022), we fine-tune the models using proximal policy optimization (PPO) (Schulman et al., 2017) on the same $N = 32$ data and use RTC as our reward model. We call this method LRTC-RL. See Appendix D for additional details.

Setup. We optimize LinEAS for 1K steps with batches of $n = 32$ (all the data we make available). As we focus on the benefit of using an end-to-end loss, we use $\gamma = 0$ for LinEAS (see Section 4.2 for γ 's impact). For Lin-Act, we

use their default settings, and set intervention strength to $\lambda = 1$. In the case of ITI-C, we performed a simple search on the λ strength and report results for the best overall setting, *i.e.*, $\lambda = 0.5$. We evaluate toxicity mitigation by intervening upon different layers, and report the best overall layer type per method, namely `*post.*layernorm` for LinEAS and `*o_proj` for ITI-C and Lin-Act, according to the Huggingface implementation of the models.

Results. Table 1 summarizes the toxicity mitigation experiments averaged over 4 generation seeds (and RTP samplings). LinEAS achieves a consistent toxicity mitigation at this low data regime. For Gemma2-2B and Qwen-1.5B we are able to match or outperform the oracle baseline LRTC-RL in terms of $\text{Tox}_{\text{RTC}}^{\text{RTP}}$. For example, LinEAS reduces Gemma2-2B toxicity by $5.5\times$. In the case of DeepSeek-7B, both Lin-Act and LinEAS achieve similar results, according to standard deviations. For the much more challenging TET dataset, we outperform ITI-C and Lin-Act on all the other models. In terms of utility, LinEAS increases PPL_{WIK} by less than +0.7 with respect to the original model, and MMLU decreases by less than 1 point. In Table 3 (Appendix A) we show that LinEAS is much more robust to the choice of layer than ITI-C and Lin-Act. Additionally, we also provide in Table 2 an analysis on a higher data regime (1024 sentences), showing that LinEAS is also reliable in that scenario. Beyond the differences in parameter sizes between ITI-C, Lin-Act and LinEAS on the one hand, and the LRTC-RL approach on the other, we also note that the compute needed to train these methods is significantly different: in the low data regime $N = 32$, estimating each method takes 4s (ITI-C), 16s (Lin-Act) leveraging closed forms, 564s (LinEAS for 1K steps) and 5940s for LRTC-RL.

4.2. Effect of Sparsity on Toxicity Mitigation

Intuitively one should only steer the smallest set of activations needed to achieve a desired goal in order to preserve utility and keep most of the model’s inference graph untouched. In this section, we explore how sparsity affects toxicity mitigation in the setup of Section 4.1 as we increase γ from 0 to 0.1. Increasing γ results in less activations being *transported*, which we measure as $\text{support} = \|(\mathbf{w} \neq \mathbf{1}) + (\mathbf{b} \neq \mathbf{0})\|_0$, *i.e.*, all those activations that are transported either by rescaling or shifts.

Results. In Figure 3 we show how $\text{Tox}_{\text{RTC}}^{\text{RTP}}$ and $\text{Tox}_{\text{RTC}}^{\text{TET}}$, as well as the utility PPL_{WIK} and MMLU, evolve as the sparse support decreases (x axis), for Qwen-7B in the low (32) data regime. We show the results of 3 sweeps of γ with different random seeds (markers), and plot the average at each γ level (line). Note that at $\gamma = 0$ the support is approximately 100%. In the case of 1K steps (reported in Table 1), one can afford reducing the support to about 1% and still maintain the toxicity mitigation values at 100% support. Interestingly,

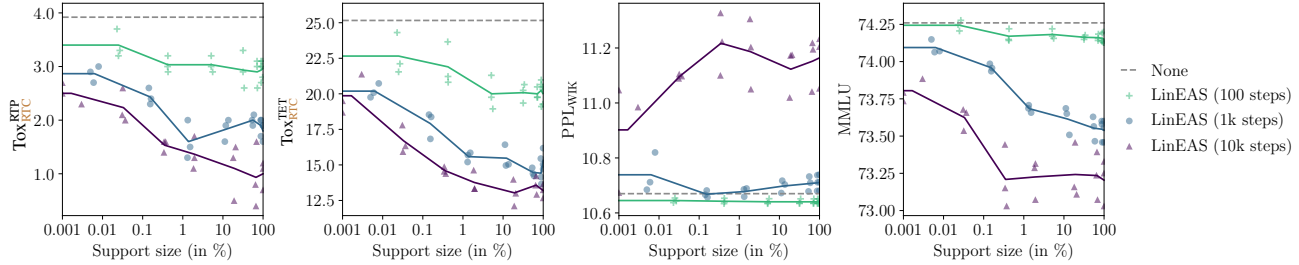


Figure 3. Sparsity improves utility while mitigating toxicity. Toxicity results on Qwen-7B using only 32 sentences, at different levels of sparsity γ that result in different support sizes (x axis). At 1K optimization steps, with a support of about 1% we maintain similar toxicity (left, center-left) while PPL_{WIK} decreases (center-right) and MMLU increases (right). Note that too long optimizations (10k steps) might harm utility, due to overfitting. Similarly, short optimizations (e.g., 100 steps) and strong sparsity leads to low conditioning (mild toxicity mitigation).

at these support values, the PPL_{WIK} and MMLU improve, validating our hypothesis that smaller supports help preserve the utility. In the figure, we also observe the effect of the optimization steps. Short optimizations (e.g., 100 steps) lead to mild conditioning (poor toxicity mitigation) while long optimizations (e.g., 10k steps) lead to a gradual degradation in utility. In Figure 9 (Appendix C) we show the same figure for the high data regime, with similar conclusions.

4.3. Composition of Interventions

We evaluate in this section the ability to compose two LinEAS maps pre-trained independently on two concepts. Our goal is to assess whether they can be composed, at the level of each activation, to induce *both* concepts. Achieving concept composition in activation steering is an open goal, and our hypothesis is that sparse and end-to-end LinEAS maps affect minimally the model, facilitating composition.

Setup. For each of the concepts *day*, *night*, *elephant*, *football* and *fishing*, we generate $N = 50$ diverse sentences using Gemma2-27B that contain that concept, to form five target (q_i). Additionally, we ask Gemma2-27B to generate 50 diverse sentences about generic situations, forming a single source distribution p . We then learn five steering maps, from p to each of the q_i distributions, using both Lin-ACT and LinEAS. For LinEAS we test all combinations of $\lambda_1 = 0, 1e^{-4}$ and $\lambda_G = 0, 1e^{-4}$, to assess the impact of sparsity. Equipped with these five concept maps, we compose them for each pair of concepts c_1, c_2 as follows: $T_\ell^{c_1 \circ c_2}(z) := T_\ell^{c_2}(T_\ell^{c_1}(z))$. Note that $T_\ell^{c_1 \circ c_2} \neq T_\ell^{c_2 \circ c_1}$. Following Rodriguez et al. (2025), we intervene on Gemma2-2B by generating 200 sentences that follow the prompt *Once upon a time* and we measure the presence of the concepts in the generations in a *LLM-as-a-judge manner*, querying Qwen-7B-Instruct. More precisely, we query about: the presence of a concept c in each generated sentence, when using the map trained with concept c ; the presence of a concept c , when using the map trained with

that concept *and* any other; the presence of both *two* concepts c_1, c_2 in the same sentence, yielding $p(c_1, c_2)$, using either $T_\ell^{c_1 \circ c_2}$ or $T_\ell^{c_2 \circ c_1}$.

Results. Figure 4.(top) plots the three probabilities described above. In particular, the right plot shows $p(c_1, c_2 | T^{c_1 \circ c_2})$, i.e., the probability of observing both concepts in the same generated sentence, using the composed map. Lin-ACT is able to generate concepts using single-concept maps (left plot) with average probability of 0.82 vs. 0.73 using LinEAS without sparsity. We also observe that increasing the sparsity (larger λ s) slightly diminishes the presence of concepts when using single-concept maps. However, we observe a drastically different picture when using *combined* maps: (middle) that probability goes from a Lin-ACT average of 0.17 to around 0.52 with LinEAS (3.1 \times increase). Most importantly, the joint presence of concepts probability (right) goes from 0.013 for Lin-ACT to 0.19 (15 \times increase) for LinEAS with *group lasso* regularization (both λ_1, λ_G used). See Appendix E for generation examples. These results show that LinEAS learns maps that are easier to compose than those from Lin-ACT. Indeed, composition of Lin-ACT maps is very brittle. While LinEAS achieves much stronger compositionality, our results show that there is still room for improvement on this important problem. We provide qualitative examples on Figure 1 and Appendix E.

4.4. Group Sparsity Trade-offs

We consider the interventions learned with Gemma2-2B for the concepts *day*, *night*, *elephant*, *football*, and *fishing*, but set both $\lambda_1 > 0$ and $\lambda_G > 0$, enforcing a sparse group regularizer. Figure 4 (bottom) shows how the proportion of intervened units, out of their entire support, is distributed across layers (post feed-forward layer norms; see Appendix F for distribution of interventions across post attention layer norms). Since we are plotting proportions of the support, differences between models in terms of the absolute number of impacted neurons are not reflected. Rather, the plot

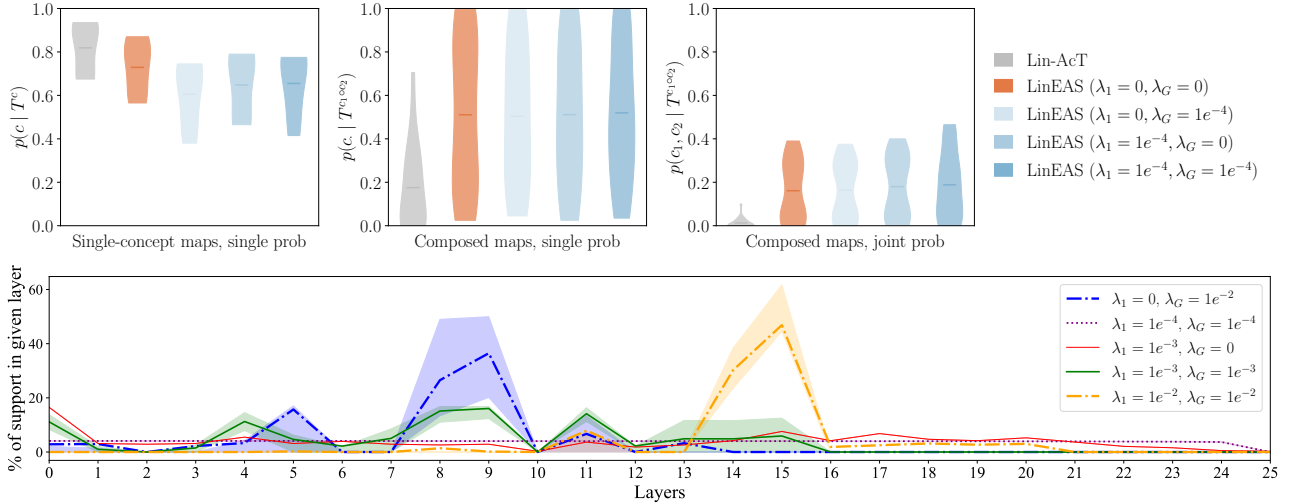


Figure 4. (Top) LinEAS obtains composable maps. We benchmark Lin-ActT and LinEAS for various regularization strengths γ on a compositional task. We train each method to model distribution shifts towards a certain concept c taking in a list of 5 concepts. **(Top-left)** We measure, using LLM as a judge, whether sentences formulated *using that trained shift* do contain that concept. We obtain for each concept a probability, that we then aggregate using violin plots. **(Top-middle)** We pick two concepts c_1 and c_2 randomly, train separately their maps, and compose them. We then measure the probability of finding c_1 , and then c_2 , in the generated content, using the composition of both maps (in both orders). **(Top-right)** We now measure the probability of finding simultaneously *both* concepts in the generations. As can be seen, the composition of LinEAS maps (learnt separately for 2 concepts) yields an average $15\times$ (right) higher probability of including both 2 concepts in the same generation, with respect to Lin-ActT, and a $3.1\times$ increase in generating at least one of the concepts (center). Interestingly, Lin-ActT obtains slightly better probability when using only single-concept maps (left), but these fail at composition. Additionally, note that sparsity in LinEAS is beneficial for compositionality, increasing the joint concept presence from 0.16 to 0.19 when using *group lasso*. In Appendix E we show qualitative results. **(Bottom) LinEAS Distribution of support across layers.** Percentage of intervened units, out of the total support, across layers (post feed-forward normalization layers) for various (λ_1, λ_G) regularization couples. Plotted values correspond to averages across interventions learned for 5 concepts (with 50% quantile range). Remarkably, these aggregate results clearly indicate that regardless of the concept, some layer positions are crucial to achieve interventions, e.g., those at positions 14 to 16 for sparse within-layer interventions, or earlier (5, 8 and 9) for dense layers.

allows to grasp how regularization, and notably group regularization, impacts layer selection. An important finding of this experiment is that we do observe, for high group regularization regimes, that very specific layers are consistently selected to induce diverse concepts. Additionally, we posit that this grouping of neurons at certain layers impacts positively efficient transfer of concepts, notably when investigating compositionality.

4.5. Steering Text-to-Image Diffusion Models

In this section, we explore uses of LinEAS to steer the text-to-image (T2I) generation of the recently proposed DMD2 model (Yin et al., 2024b), used here with a single diffusion step, *i.e.*, as a GAN. As in (Rodriguez et al., 2025), we modulate the strength of LinEAS applied to all `layernorm` layers by introducing a scale $0 \leq \lambda \leq 1$ when applying interventions T_ℓ in equation 5, using $T_\ell^\lambda(z) := (1-\lambda)z + \lambda T_\ell(z)$. Intuitively $\lambda = 0$ results in no intervention, while $\lambda = 1$ carries out a full LinEAS shift, any value in between reflecting a gradual change. We train LinEAS and Lin-ActT to induce different styles (anime, art-nouveau, cyberpunk, sketch, and

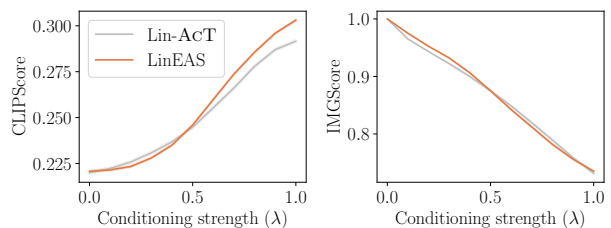


Figure 5. LinEAS improves conditioning of T2I diffusion over Lin-ActT. LinEAS can induce styles better, achieving a CLIPScore of 0.30, where Lin-ActT ≈ 0.29 (left). Both maintain similar fidelity to the untouched model (IMGScore, right). Error bars are barely discernible. See qualitative results in Figure 7.

watercolor) on the same setup described by Rodriguez et al. (2025). As in Section 4.1, we use 32 samples for each of the source and the target distribution. We train LinEAS for 1000 steps with batch size 4, AdamW, a learning rate of $5e^{-4}$, and γ of $1e^{-4}$. We provide additional implementation details in Appendix H.

Results. We compare LinEAS and Lin-ActT on style gen-



Figure 6. Generations using DMD2 (Yin et al., 2024b) with Lin-ACT (above) or LinEAS (below) for the prompts *A wolf tracking prey* (left) and *A caterpillar crawling on a leaf* (right). In each image, we show generations at $\lambda = [0, 0.5, 0.75, 1.0]$ from left to right. Several concepts are induced, shown below each image pair. Note the much better quality of the LinEAS generations.



Figure 7. Generations using DMD2 (Yin et al., 2024b) with Lin-ACT (above) or LinEAS (below) for various prompts while inducing styles *art-nouveau* (left) and *cyberpunk* (right). LinEAS outperforms Lin-ACT in at style induction, as also shown quantitatively in Figure 5.

eration, and we measure: (1) **CLIPScore** (Hessel et al., 2021), the cosine similarity between the CLIP (Radford et al., 2021) embedding of the generated images at a given λ and the embedding of the style prompt and (2) **IMGScore**, the cosine similarity between the embedding of the generated images at $\lambda > 0$ and that of the generations at $\lambda = 0$. CLIPScore assesses whether the generations are truthful

to the desired style, and IMGScore assesses whether the generated images maintain the content generated without intervention. LinEAS achieves stronger conditioning with CLIPScore = 0.30, for 0.29 using Lin-ACT. Although the difference seems small, it results in a large quality difference between both, which can be appreciated in Figure 7. To further showcase the data efficiency and versatility of our method at conditioning T2I diffusion, we prompt a Gemma2-27B to generate 32 sentences, with which we learn LinEAS maps for each of the styles: Salvador Dalí, Robots, Fantasy, Kid’s painting, Retro 3D graphics, Flower power and Ukiyo-e, and provide qualitative results in Figure 6.

5. Conclusion

We proposed LinEAS, a novel framework to learn lightweight interventions on activations to steer model generation towards a desired property, with safety applications, such as avoiding toxic outputs, or style changes, both for LLM and text-to-image diffusion. Our approach learns a set of univariate maps that reshape a source to a target distribution with an improved loss that yields improved controllability and robustness. Unlike previous methods, such as (Rodriguez et al., 2025; Li et al., 2024), which require local adjustments and manual layer selection, our method optimizes the transformation globally in an end-to-end fashion. This approach also allows for the incorporation of flexible regularizers, such group-sparse and sparse, allowing for the automatic selection of both layers and neurons on which to intervene upon. Our method is cheap to train and use, and effective with very low data (32 exemplar sentences from both source and target sets), and achieves state-of-the-art toxicity

reduction on the TET and RTP datasets, while maintaining perplexity and MMLU performance on all the tested models (Gemma2-2B, DeepSeek-7B, Qwen-1.5B and Qwen-7B). We demonstrate interesting tradeoffs arising from enforcing sparsity of these transforms and much improved compositional properties. We also show that LinEAS interventions can be applied using variable strength in a text-to-image application. The code will be publicly available shortly.

Impact Statement

This paper presents work whose goal is to advance the field of Machine Learning. There are many potential societal consequences of our work, none which we feel must be specifically highlighted here.

References

- Adams, C., Sorensen, J., Elliott, J., Dixon, L., McDonald, M., nithum, and Cukierski, W. Toxic comment classification challenge, 2017. URL <https://kaggle.com>.
- Belloni, A. and Chernozhukov, V. Least squares after model selection in high-dimensional sparse models. 2013.
- Brown, T., Mann, B., Ryder, N., Subbiah, M., Kaplan, J. D., Dhariwal, P., Neelakantan, A., Shyam, P., Sastry, G., Askell, A., et al. Language models are few-shot learners. *Advances in neural information processing systems*, 33: 1877–1901, 2020.
- Chen, X., Fang, H., Lin, T.-Y., Vedantam, R., Gupta, S., Dollár, P., and Zitnick, C. L. Microsoft coco captions: Data collection and evaluation server. *arXiv preprint arXiv:1504.00325*, 2015.
- Chzen, E., Hebiri, M., and Salmon, J. On lasso refitting strategies. *Bernoulli*, 25(4A):3175–3200, 2019.
- Gehman, S., Gururangan, S., Sap, M., Choi, Y., and Smith, N. A. Realtotoxicityprompts: Evaluating neural toxic degeneration in language models. *arXiv preprint arXiv:2009.11462*, 2020.
- Geiger, A., Wu, Z., Potts, C., Icard, T., and Goodman, N. Finding alignments between interpretable causal variables and distributed neural representations. In *Causal Learning and Reasoning*, pp. 160–187. PMLR, 2024.
- Hendrycks, D., Burns, C., Basart, S., Zou, A., Mazeika, M., Song, D., and Steinhardt, J. Measuring massive multitask language understanding. *Proceedings of the International Conference on Learning Representations (ICLR)*, 2021.
- Hessel, J., Holtzman, A., Forbes, M., Le Bras, R., and Choi, Y. Clipscore: A reference-free evaluation metric for image captioning. In *Proceedings of the 2021 Conference on Empirical Methods in Natural Language Processing*, pp. 7514–7528, 2021.
- Ho, J. and Salimans, T. Classifier-free diffusion guidance. *arXiv preprint arXiv:2207.12598*, 2022.
- Huu-Tien, D., Pham, T.-T., Thanh-Tung, H., and Inoue, N. On effects of steering latent representation for large language model unlearning. *arXiv preprint arXiv:2408.06223*, 2024.
- Li, K., Patel, O., Viégas, F., Pfister, H., and Wattenberg, M. Inference-time intervention: Eliciting truthful answers from a language model. *Advances in Neural Information Processing Systems*, 36, 2024.
- Lin, S., Hilton, J., and Evans, O. Truthfulqa: Measuring how models mimic human falsehoods. *arXiv preprint arXiv:2109.07958*, 2021.
- Liu, S., Ye, H., Xing, L., and Zou, J. In-context vectors: Making in context learning more effective and controllable through latent space steering. *arXiv preprint arXiv:2311.06668*, 2023.
- Logacheva, V., Dementieva, D., Ustyantsev, S., Moskovskiy, D., Dale, D., Krotova, I., Semenov, N., and Panchenko, A. ParaDetox: Detoxification with parallel data. In *Proceedings of the 60th Annual Meeting of the Association for Computational Linguistics (Volume 1: Long Papers)*, pp. 6804–6818, Dublin, Ireland, May 2022. Association for Computational Linguistics. URL <https://aclanthology.org/2022.acl-long.469>.
- Luo, M., Wong, J., Trabucco, B., Huang, Y., Gonzalez, J. E., Chen, Z., Salakhutdinov, R., and Stoica, I. Stylus: Automatic adapter selection for diffusion models. In *The Thirty-eighth Annual Conference on Neural Information Processing Systems*, 2024. URL <https://openreview.net/forum?id=30dq2tGSpp>.
- Luong, T. S., Le, T.-T., Van, L. N., and Nguyen, T. H. Realistic evaluation of toxicity in large language models, 2024.
- Ouyang, L., Wu, J., Jiang, X., Almeida, D., Wainwright, C., Mishkin, P., Zhang, C., Agarwal, S., Slama, K., Ray, A., et al. Training language models to follow instructions with human feedback. *Advances in Neural Information Processing Systems*, 35:27730–27744, 2022.
- Rabin, J., Peyré, G., Delon, J., and Bernot, M. Wasserstein barycenter and its application to texture mixing. In *Scale Space and Variational Methods in Computer Vision: Third International Conference, SSVM 2011, Ein-Gedi, Israel, May 29–June 2, 2011, Revised Selected Papers 3*, pp. 435–446. Springer, 2012.

- Radford, A., Kim, J. W., Hallacy, C., Ramesh, A., Goh, G., Agarwal, S., Sastry, G., Askell, A., Mishkin, P., Clark, J., Krueger, G., and Sutskever, I. Learning transferable visual models from natural language supervision, 2021.
- Rimsky, N., Gabrieli, N., Schulz, J., Tong, M., Hubinger, E., and Turner, A. M. Steering llama 2 via contrastive activation addition. *arXiv preprint arXiv:2312.06681*, 2023.
- Rodriguez, P., Blaas, A., Klein, M., Zappella, L., Apostoloff, N., Cuturi, M., and Suau, X. Controlling language and diffusion models by transporting activations, 2025.
- Santambrogio, F. Optimal transport for applied mathematicians. *Birkäuser, NY*, 55(58-63):94, 2015.
- Scalena, D., Sarti, G., and Nissim, M. Multi-property steering of large language models with dynamic activation composition. *arXiv preprint arXiv:2406.17563*, 2024.
- Schulman, J., Wolski, F., Dhariwal, P., Radford, A., and Klimov, O. Proximal policy optimization algorithms. *arXiv preprint arXiv:1707.06347*, 2017.
- Sclar, M., Choi, Y., Tsvetkov, Y., and Suhr, A. Quantifying language models’ sensitivity to spurious features in prompt design or: How i learned to start worrying about prompt formatting. *ICLR*, 2024.
- Simon, N., Friedman, J., Hastie, T., and Tibshirani, R. A sparse-group lasso. *Journal of computational and graphical statistics*, 22(2):231–245, 2013.
- Suau, X., Zappella, L., and Apostoloff, N. Self-conditioning pre-trained language models. In *International Conference on Machine Learning*, pp. 4455–4473. PMLR, 2022.
- Suau, X., Delobelle, P., Metcalf, K., Joulin, A., Apostoloff, N., Zappella, L., and Rodriguez, P. Whispering experts: Neural interventions for toxicity mitigation in language models. In *Forty-first International Conference on Machine Learning*, 2024. URL <https://openreview.net/forum?id=2P6GVfSrfZ>.
- Turner, A., Thiergart, L., Udell, D., Leech, G., Mini, U., and MacDiarmid, M. Activation addition: Steering language models without optimization. *arXiv preprint arXiv:2308.10248*, 2023.
- van der Weij, T., Poesio, M., and Schoots, N. Extending activation steering to broad skills and multiple behaviours. *arXiv preprint arXiv:2403.05767*, 2024.
- Wei, J., Bosma, M., Zhao, V., Guu, K., Yu, A. W., Lester, B., Du, N., Dai, A. M., and Le, Q. V. Finetuned language models are zero-shot learners. In *International Conference on Learning Representations*, 2022.
- Wikimedia, F. Wikimedia downloads. URL <https://dumps.wikimedia.org>.
- Wu, Z., Arora, A., Wang, Z., Geiger, A., Jurafsky, D., Manning, C. D., and Potts, C. ReFT: Representation fine-tuning for language models. 2024. URL arxiv.org/abs/2404.03592.
- Yin, F., Ye, X., and Durrett, G. Lofit: Localized fine-tuning on llm representations. *NeurIPS*, 2024a.
- Yin, T., Gharbi, M., Park, T., Zhang, R., Shechtman, E., Durand, F., and Freeman, W. T. Improved distribution matching distillation for fast image synthesis. In *NeurIPS*, 2024b.
- Yoon, J. and Hwang, S. J. Combined group and exclusive sparsity for deep neural networks. In Precup, D. and Teh, Y. W. (eds.), *Proceedings of the 34th International Conference on Machine Learning*, volume 70 of *Proceedings of Machine Learning Research*, pp. 3958–3966. PMLR, 06–11 Aug 2017. URL <https://proceedings.mlr.press/v70/yoon17a.html>.
- Zhang, H., Wang, X., Li, C., Ao, X., and He, Q. Controlling large language models through concept activation vectors. *arXiv preprint arXiv:2501.05764*, 2025.
- Zou, A., Phan, L., Chen, S., Campbell, J., Guo, P., Ren, R., Pan, A., Yin, X., Mazeika, M., Dombrowski, A.-K., et al. Representation engineering: A top-down approach to ai transparency. *arXiv preprint arXiv:2310.01405*, 2023.

A. Toxicity Mitigation (extended results)

In Table 2 we show results analogous to those in Table 1 but in a higher data regime, *i.e.*, using 1024 sentences per set.

Additionally, in Table 3, we show how the different activation steering methods perform in the setting of Section 4.1, when intervening different layer types (namely `. *post_.*_layernorm` and `. *o_proj` of the models’ Huggingface implementation). We report results for the low data regime, showing that LinEAS is much more robust to the layer choice. Indeed, for `. *post_.*_layernorm` and models DeepSeek-7B and Qwen-1.5B, ITI-C and Lin-ACT induce a toxicity slightly higher than the original one (marked in red).

Model	method	# par (M)	Tox _{RTP} ^{RTP} (↓)	Tox _{RTP} ^{TET} (↓)	PPL _{WIK} (↓)	MMLU (↑)
Gemma2-2B	None	-	4.00 _{0.45}	13.39 _{1.42}	14.79 _{0.00}	53.03 _{0.00}
	LRTC-RL	0.8	0.50 _{0.44}	1.68 _{0.01}	15.78 _{0.19}	52.45 _{0.54}
	ITI-c	0.06	0.30 _{0.26}	2.68 _{0.43}	14.65 _{0.06}	52.04 _{0.17}
	Lin-ACT	0.12	1.07 _{0.52}	6.08 _{0.67}	14.85 _{0.04}	52.36 _{0.11}
	LinEAS	0.24	0.95 _{0.26}	3.46 _{0.44}	15.82 _{0.02}	51.28 _{0.08}
DeepSeek-7B	None	-	4.30 _{0.70}	18.62 _{0.51}	8.49 _{0.00}	48.31 _{0.00}
	LRTC-RL	1.97	0.90 _{0.30}	1.95 _{0.00}	8.80 _{0.03}	47.28 _{0.58}
	ITI-c	0.13	1.77 _{0.40}	10.70 _{1.14}	7.79 _{0.02}	48.20 _{0.15}
	Lin-ACT	0.25	1.42 _{0.43}	9.39 _{0.34}	8.77 _{0.01}	47.74 _{0.17}
	LinEAS	0.25	1.70 _{0.14}	9.49 _{0.52}	8.53 _{0.04}	48.01 _{0.04}
Qwen-1.5B	None	-	3.00 _{0.54}	23.09 _{0.67}	13.67 _{0.00}	60.95 _{0.00}
	LRTC-RL	0.54	0.67 _{0.40}	3.93 _{0.01}	13.91 _{0.09}	60.70 _{0.19}
	ITI-c	0.043	1.60 _{0.10}	15.50 _{0.81}	12.53 _{0.04}	60.73 _{0.21}
	Lin-ACT	0.086	0.95 _{0.38}	11.61 _{1.43}	14.06 _{0.03}	59.82 _{0.22}
	LinEAS	0.086	0.90 _{0.26}	12.56 _{0.70}	14.20 _{0.04}	59.21 _{0.16}
Qwen-7B	None	-	3.92 _{0.59}	25.16 _{0.92}	10.67 _{0.00}	74.26 _{0.00}
	LRTC-RL	1.26	1.50 _{0.36}	5.28 _{0.00}	11.03 _{0.05}	73.91 _{0.10}
	ITI-c	0.10	2.33 _{0.76}	18.18 _{2.00}	9.66 _{0.04}	74.19 _{0.10}
	Lin-ACT	0.20	1.65 _{0.26}	13.60 _{0.99}	10.80 _{0.02}	73.60 _{0.07}
	LinEAS	0.20	1.52 _{0.33}	13.92 _{0.54}	10.89 _{0.14}	73.37 _{0.07}

Table 2. Toxicity mitigation on the RTP and TET datasets. We report results at low ($N = 1024$ sentences to estimate the interventions) data regime. We used 10k optimization steps, with minibatches of size $n = 32$. In the high-data regime, Lin-ACT achieves an outstanding 0.68 Tox_{RTP}^{RTP} for Gemma2-2B. However, this method struggles at reducing toxicity for the other models. Conversely, LinEAS achieves similar (Gemma2-2B) or better (other models) RTP toxicity mitigation than in the low data setup, and with better MMLU than Lin-ACT for all models. Similarly, LinEAS outperforms all other methods on TET toxicity mitigation by a large margin.

End-to-end Learning of Sparse Interventions on Activations to Steer Generation

Model	Method	Layer	Data	λ	Tox _{RTP} ^{RTP} (\downarrow)	Tox _{RTP} ^{TET} (\downarrow)	PPL _{WIK} (\downarrow)	MMLU (\uparrow)
Gemma2-2B	None	.*post.*_layernorm	-	-	4.00 _{0.45}	13.39 _{1.42}	14.79 _{0.00}	53.03 _{0.00}
	ITI-C	.*post.*_layernorm	32	1.0	2.38 _{0.91}	10.00 _{0.57}	13.89 _{0.13}	52.92 _{0.14}
	Lin-ACT	.*post.*_layernorm	32	1.0	1.35 _{0.17}	7.32 _{1.16}	15.08 _{0.13}	51.52 _{0.32}
	LinEAS	.*post.*_layernorm	32	1.0	0.73 _{0.10}	4.02 _{0.68}	15.46 _{0.21}	52.22 _{0.40}
DeepSeek-7B	None	.*post.*_layernorm	-	-	4.30 _{0.70}	18.62 _{0.51}	8.49 _{0.00}	48.31 _{0.00}
	ITI-C	.*post.*_layernorm	32	1.0	7.23 _{0.76}	28.13 _{2.45}	8.85 _{0.40}	45.82 _{1.15}
	Lin-ACT	.*post.*_layernorm	32	1.0	5.62 _{0.25}	24.29 _{1.46}	9.37 _{0.20}	45.95 _{0.04}
	LinEAS	.*post.*_layernorm	32	1.0	2.30 _{0.14}	12.09 _{0.83}	8.38 _{0.05}	48.13 _{0.07}
Qwen-1.5B	None	.*post.*_layernorm	-	-	3.00 _{0.54}	23.09 _{0.67}	13.67 _{0.00}	60.95 _{0.00}
	ITI-C	.*post.*_layernorm	32	1.0	2.62 _{0.30}	19.35 _{1.52}	13.23 _{0.17}	60.37 _{0.24}
	Lin-ACT	.*post.*_layernorm	32	1.0	2.75 _{0.68}	25.51 _{1.79}	16.33 _{0.85}	57.66 _{0.56}
	LinEAS	.*post.*_layernorm	32	1.0	1.07 _{0.46}	12.70 _{0.74}	14.10 _{0.07}	59.97 _{0.16}
Qwen-7B	None	.*post.*_layernorm	-	-	3.92 _{0.59}	25.16 _{0.92}	10.67 _{0.00}	74.26 _{0.00}
	ITI-C	.*post.*_layernorm	32	1.0	2.88 _{0.60}	19.41 _{1.11}	9.69 _{0.07}	74.13 _{0.05}
	Lin-ACT	.*post.*_layernorm	32	1.0	2.77 _{0.39}	20.57 _{1.36}	11.64 _{0.24}	72.21 _{0.08}
	LinEAS	.*post.*_layernorm	32	1.0	1.88 _{0.19}	15.39 _{0.60}	10.83 _{0.25}	73.56 _{0.07}
Gemma2-2B	None	.*o_proj	-	-	4.00 _{0.45}	13.39 _{1.42}	14.79 _{0.00}	53.03 _{0.00}
	ITI-C	.*o_proj	32	0.5	1.17 _{0.60}	7.15 _{0.92}	14.00 _{0.11}	52.78 _{0.23}
	Lin-ACT	.*o_proj	32	1.0	1.60 _{0.32}	7.76 _{0.39}	14.78 _{0.12}	52.43 _{0.57}
	LinEAS	.*o_proj	32	1.0	2.10 _{0.34}	8.78 _{0.56}	14.72 _{0.16}	53.27 _{0.41}
DeepSeek-7B	None	.*o_proj	-	-	4.30 _{0.70}	18.62 _{0.51}	8.49 _{0.00}	48.31 _{0.00}
	ITI-C	.*o_proj	32	0.5	2.83 _{0.40}	15.18 _{2.00}	7.71 _{0.07}	48.47 _{0.25}
	Lin-ACT	.*o_proj	32	1.0	2.23 _{0.69}	11.08 _{0.76}	8.67 _{0.03}	47.71 _{0.27}
	LinEAS	.*o_proj	32	1.0	2.30 _{0.48}	8.46 _{0.54}	8.61 _{0.06}	46.35 _{0.37}
Qwen-1.5B	None	.*o_proj	-	-	3.00 _{0.54}	23.09 _{0.67}	13.67 _{0.00}	60.95 _{0.00}
	ITI-C	.*o_proj	32	0.5	1.87 _{0.21}	18.16 _{0.62}	12.39 _{0.09}	60.88 _{0.08}
	Lin-ACT	.*o_proj	32	1.0	1.50 _{0.35}	13.88 _{1.72}	13.88 _{0.16}	60.09 _{0.25}
	LinEAS	.*o_proj	32	1.0	1.50 _{0.29}	12.03 _{0.71}	14.04 _{0.10}	59.53 _{0.17}
Qwen-7B	None	.*o_proj	-	-	3.92 _{0.59}	25.16 _{0.92}	10.67 _{0.00}	74.26 _{0.00}
	ITI-C	.*o_proj	32	0.5	2.97 _{0.21}	20.68 _{2.21}	9.56 _{0.02}	74.20 _{0.07}
	Lin-ACT	.*o_proj	32	1.0	2.25 _{0.13}	16.04 _{0.95}	10.77 _{0.09}	73.56 _{0.08}
	LinEAS	.*o_proj	32	1.0	2.00 _{0.18}	13.58 _{0.76}	12.52 _{0.07}	71.34 _{0.10}

Table 3. **LinEAS is more robust to the layer choice.** Toxicity mitigation on the RTP and TET datasets, intervening on .*post.*_layernorm and .*o_proj layers. We report results at low (32 sentences) regime, showing in **bold** the best toxicity result per model. When intervening on .*post.*_layernorm, both ITI-C and Lin-ACT show poorer performance, specially for DeepSeek-7B and Qwen-1.5B, where the toxicity goes even above the original one (in red). For .*o_proj, ITI-C and Lin-ACT perform better. Overall, LinEAS shows strong robustness to the layer choice.

B. Order of Magnitude of Interventions Parameters

To inform the scale of regularization terms, we plot descriptive statistics of the values of **w** and **b**, layer by layer.

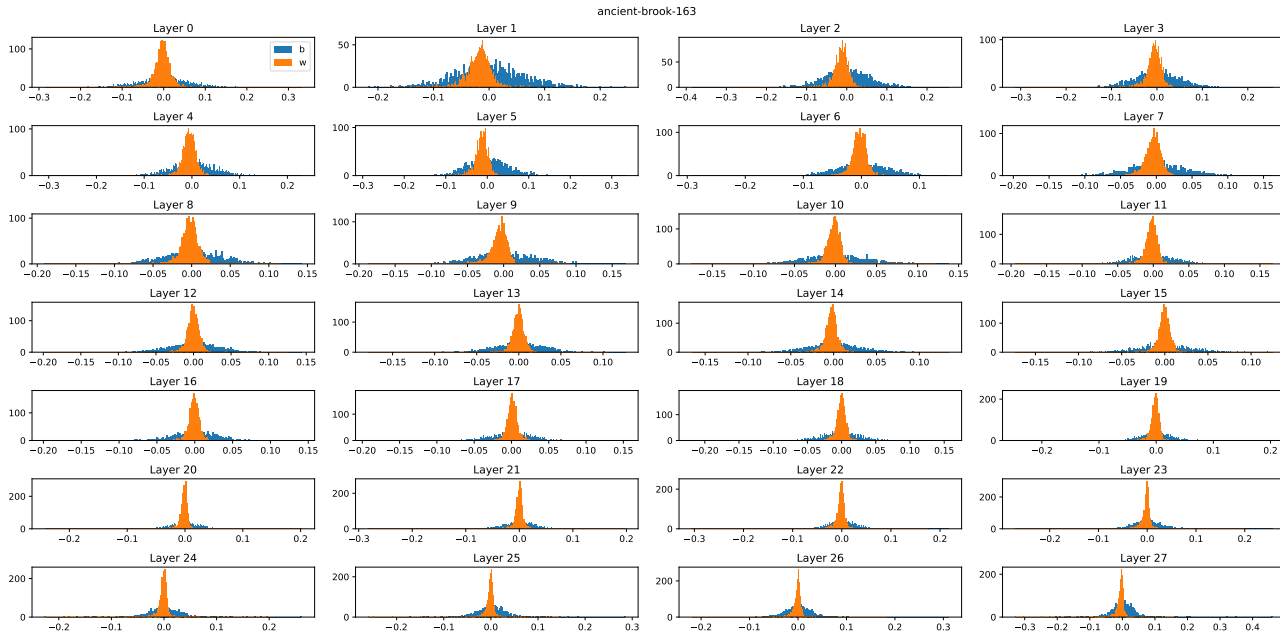


Figure 8. Distribution, layer by layer, of recentered scale parameters w and b biases, for a converged run of LinEAS, intervening on the 28 intervened layers of Gemma2-2B.

C. Effect of Sparsity on Toxicity Mitigation (extended results)

We complement the results shown in Figure 3, this time measuring the effect of sparsity on toxicity mitigation when the transport maps are optimized with 1024 (source and target) sentences. The results and trends discussed in Figure 3 also hold in this setup with more data.

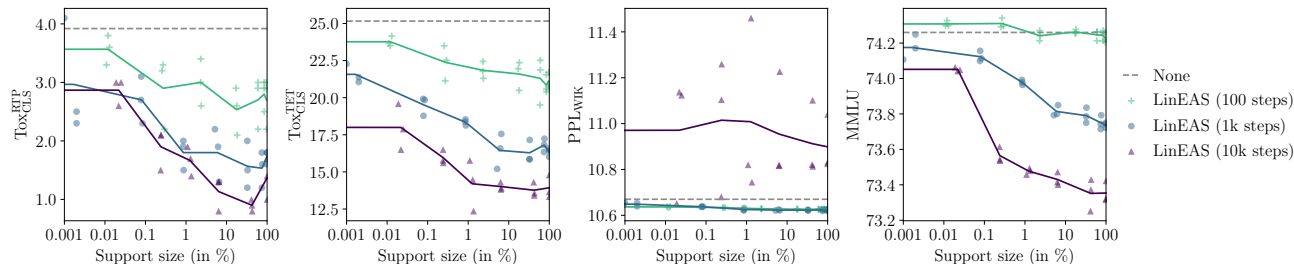


Figure 9. **Sparsity improves utility while mitigating toxicity, also in high data regime.** Toxicity results on Qwen-7B using 1024 sentences, at different levels of sparsity γ that result in different support sizes (x axis). With a support of 1%-5% we maintain similar toxicity (left, center-left) while PPL_{WIK} decreases (center-right) and MMLU increases (right). Note that too long optimizations (30k steps) might harm utility, due to overfitting. Similarly, short optimizations (e.g., 300 steps) and strong sparsity leads to low conditioning (mild toxicity mitigation).

D. RLHF Implementation Details

We perform parameter-efficient adaptation of our baseline models with Huggingface’s implementation of LoRA in their PEFT library and Huggingface’s implementation of the PPO reinforcement learning algorithm in their TRL library. For each sample size in Table 1, we performed an hyperparameter search and chose the hyperparameters that yielded best validation toxicity scores at a perplexity close to LinEAS. We instantiate the reward model with the Roberta toxicity classifier from Logacheva et al. (2022) used for evaluation (RTC in Table 1); we use the base model without LoRA weights as the reference model and the LoRA model as the policy; we add an off-the-shelf value head from TRL to the policy to estimate the value function. We follow the original LoRA implementation and only fine-tune $\{k, q, v, o\}$ -proj layers while keeping the

MLPs frozen. The summary of hyperparameters can be found in Table 4.

Hyperparameter	Values	Best 32 Samples	Best 1024 Samples
global_epochs	{10, 15, 20}	10	15
ppo_epochs	{1, 10, 20, 50}	20	20
learning_rate	{ 10^{-4} , $5 * 10^{-5}$, 10^{-5} }	10^{-5}	10^{-5}
batch_size	{32, 64, 128}	32	128
mini_batch_size	{16, 32, 64}	32	64
lora_rank	{2, 4, 8}	2	2

Table 4. List of hyper-parameters used to train PPO for 32 and 1024 samples. Unless otherwise specified, we use TRL’s defaults. We could not use a mini-batch size greater than 64 due to memory constraints. We did not use gradient accumulation. We found the learning_rate and global_epochs to be the most important hyper-parameters. Low learning rate for few epochs leads to underfitting while high learning rate for many epochs tends to overfit.

E. Composition of Interventions: Qualitative Results

We show qualitative results using composed maps as detailed in Section 4.3. In Table 5 and Table 6 we include generations that were marked as containing both concepts using LLM-as-a-judge (Qwen-7B-Instruct). We compare Lin-ACT and LinEAS (with $\gamma = 1e^{-4}$).

Table 5. Generations inducing both concepts *Fishing, Elephant*. Only the provided 2 generations for Lin-ACT were marked as containing both concepts using LLM-as-a-judge, out of 200. Conversely, 25 sentences generated by LinEAS contain both concepts. Note the stark difference in quality, LinEAS achieves high quality generations with composition.

Composition	Method	Generation
Fishing ◦ Elephant	Lin-ACT	Once upon a time, the Tuffa as the bull elephant’s foot as she made a small &strong>putty as the water as she nosed the bank of the river as the water, as the sun as the swaying on the water as she stood in the shallows, the as the water [...]
Fishing ◦ Elephant	Lin-ACT	Once upon a time, a large, gray, as it was the bull as it snorted in the water as it struggled to break the line of the bank as it thrashed in the water, a small stream of water, as it made a final sprint, as the water, as it snorted noisily, the water as the river [...]
Fishing ◦ Elephant	LinEAS	Once upon a time, a man was fishing in the river when he saw a beautiful, pink baby elephant walking towards him. The elephant was thirsty and the man offered him a drink of water. The elephant was grateful and splashed some water on the man’s face.
Fishing ◦ Elephant	LinEAS	Once upon a time, a huge elephant’s tusk broke the water, his trunk splashing in the shallow river. ”Hup!” he called, his tail swished against the muddy bank. I watched from the shore, my fishing rod dangling in the water.
Fishing ◦ Elephant	LinEAS	Once upon a time, the elephant’s trunk broke the water, his massive body rising and disappearing. The jungle rumbled in the distance, their long tusks scraping against the mud. It was a young calf, its small, wet back. The fisherman sat on the bank, his net swinging lazily in the shallow water. A small fish

Table 6. Generations inducing both concepts *Night, Football*.

Composition	Method	Generation
Night ◦ Football	Lin-ACT	Once upon a time, a little girl’s dream came true. It was the first night of the 2013-14 season and the young forward had just scored her first goal for the first team. The ball had nestled in the net in the 15th minute of the game, and the 16-year-old couldn’t believe her luck.
Night ◦ Football	Lin-ACT	Once upon a time, there was a man who was so determined to win the game, he went out to play in the rain. It was a cold, wet night, and the rain was pouring down, but the man didn’t let it dampen his spirits. He was out to win the game, and he knew that he had to make a late, late goal to seal the victory.
Night ◦ Football	Lin-ACT	Once upon a time, I was a happy camper. I was in the middle of a long drive through the woods, the sound of the wind whistling through the trees. The air was cool and the sun was setting, casting a warm glow over the forest. As I drove, I couldn’t help but feel a sense of excitement. I had just won the race to the finish line, the ball bouncing off the net, and the ball was heading for the goal.
Night ◦ Football	LinEAS	Once upon a time, in the night, the lights of the field illuminated the players. The crowd roared in excitement, their voices echoing off the stands. It was the final whistle, and the opposing team celebrated, their coach shouting with joy.
Night ◦ Football	LinEAS	Once upon a time, the “ <i>Let’s go Rangers!</i> ” could be heard through the dark, cold night. The home crowd cheered and the ball flew past the goal, sending a shower of confetti into the air.
Night ◦ Football	LinEAS	Once upon a time, the sun set on the field of grass. The opposing teams were locked in a fierce battle, the crowd roaring with excitement. It was the opening goal, and the referee blew his whistle, signaling the end of the game.

F. Distribution of Interventions: Post Attention Layer Norms

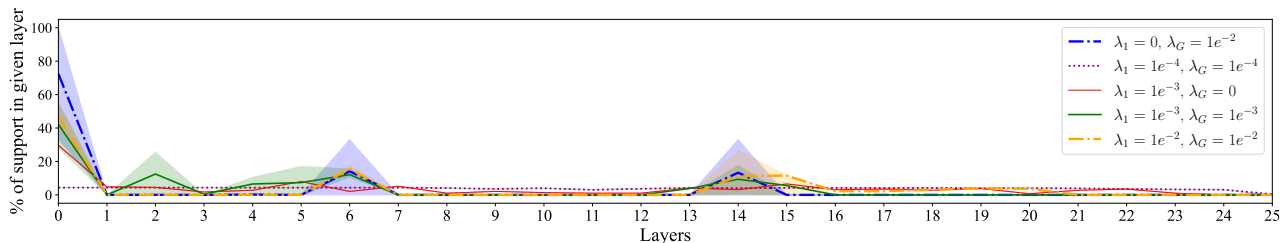


Figure 10. **LinEAS Distribution of support across layers.** Percentage of intervened units, out of the total support, across layers (post attention normalization layers) for various (λ_1, λ_G) regularization couples. Plotted values correspond to averages across interventions learned for 5 concepts (with 50% quantile range). These aggregate results, in line with those in Figure 4.(top), clearly indicate that regardless of the concept, some layer positions are crucial to achieve interventions.

G. Additional Experiment: Inducing Truthfulness in LLMs

In this section, we complement and corroborate our insights from the experiments on toxicity mitigation in Section 4.1 with additional experiments on inducing truthfulness in LLMs, using the TruthfulQA benchmark (Lin et al., 2021). In particular, we investigate how well LinEAS achieves to induce truthfulness on this benchmark in comparison to Lin-ACT, its strongest activation steering competitor from Section 4.1.

For LinEAS, we apply the intervention again to the post layernorm layers, while for Lin-ACT, we apply them to all layernorm layers as this was reported as optimal for Lin-ACT for TruthfulQA experiments in Rodriguez et al. (2025). We use 2-fold cross-validation on the 817 questions of the multiple choice part of the benchmark and learn the intervention on

the concatenation of training fold questions concatenated with either incorrect (source) or correct (target) multiple-choice answer options. We report both MC1 and MC2 of TruthfulQA, and monitor overfitting on the TruthfulQA task by also evaluating MMLU 5-shot accuracy (Hendrycks et al., 2021).

The results can be found in Table 7. We see that both methods can successfully induce truthfulness when presented with enough samples to learn the interventions, increasing the accuracy by up to almost 5% (7%) on MC1 (MC2) in the high sample regime when 1024 samples are available. Overall the highest increases can be achieved with Lin-ACT, but only for the high sample regime. In the low sample regime, where only 32 samples are available, Lin-ACT tends to fail catastrophically: either it gets lower accuracies on MC1 and MC2 than even the unintervened model (Qwen-7B, Qwen-1.5B), or it fails completely on MMLU (Gemma2-2B). LinEAS on the other hand does well also in this low sample regime, and achieves second best overall performance on the Qwen models with only 32 samples available to learn interventions.

Model	Samples	Method	MC1 Acc. (%) (↑)	MC2 Acc. (%) (↑)	MMLU (↑)
Qwen-7B	-	None	37.82 _{0.00}	52.14 _{0.00}	74.26 _{0.00}
	32	Lin-ACT	32.17 _{0.66}	47.69 _{0.87}	59.22 _{1.74}
		LinEAS	40.10 _{0.37}	55.74 _{0.31}	73.88 _{0.07}
	1024	Lin-ACT	42.59 _{0.50}	58.92 _{0.82}	73.79 _{0.14}
		LinEAS	39.56 _{0.13}	55.20 _{0.15}	73.88 _{0.02}
	Qwen-1.5B	-	None	30.23 _{0.00}	43.70 _{0.00}
32		Lin-ACT	27.22 _{1.38}	42.64 _{3.17}	32.10 _{1.95}
		LinEAS	32.26 _{0.65}	46.07 _{0.63}	60.34 _{0.12}
1024		Lin-ACT	32.90 _{0.36}	47.17 _{0.61}	60.17 _{0.18}
		LinEAS	31.77 _{0.11}	45.31 _{0.20}	60.41 _{0.01}
Gemma2-2B		-	None	21.18 _{0.00}	33.05 _{0.00}
	32	Lin-ACT	24.94 _{1.15}	40.95 _{1.29}	27.59 _{1.09}
		LinEAS	24.21 _{0.85}	38.09 _{1.14}	52.08 _{0.16}
	1024	Lin-ACT	25.65 _{0.53}	39.73 _{0.49}	51.40 _{0.17}
		LinEAS	23.82 _{0.19}	37.80 _{0.53}	52.37 _{0.05}

Table 7. Results on TruthfulQA. We report results at low data (32 samples to estimate the interventions) and high (1024 samples) regimes. Results are averaged over five random seeds.

H. Additional details and results on text to image generation

H.1. Additional qualitative results with LLM-generated prompts

We extend here the qualitative results inducing several styles, comparing Lin-ACT and LinEAS, showing several examples in Figures 11 to 19. Both the diversity and (human) perceptual quality of the generations is higher with LinEAS. We observe stark differences between both methods’ generations. Lin-ACT converges to more similar color palettes for each style (e.g., dark blue and purple for *Robot*) while LinEAS generates more crisp and diverse images. For example, *Kid’s drawing* leads to blurry and shapeless images with Lin-ACT, while LinEAS obtains accurate and crisp images. We would like to remark that both Lin-ACT and LinEAS perform a 1d affine projection of the activations. The benefit of learning these projections end-to-end with LinEAS is clearly visible in these examples.

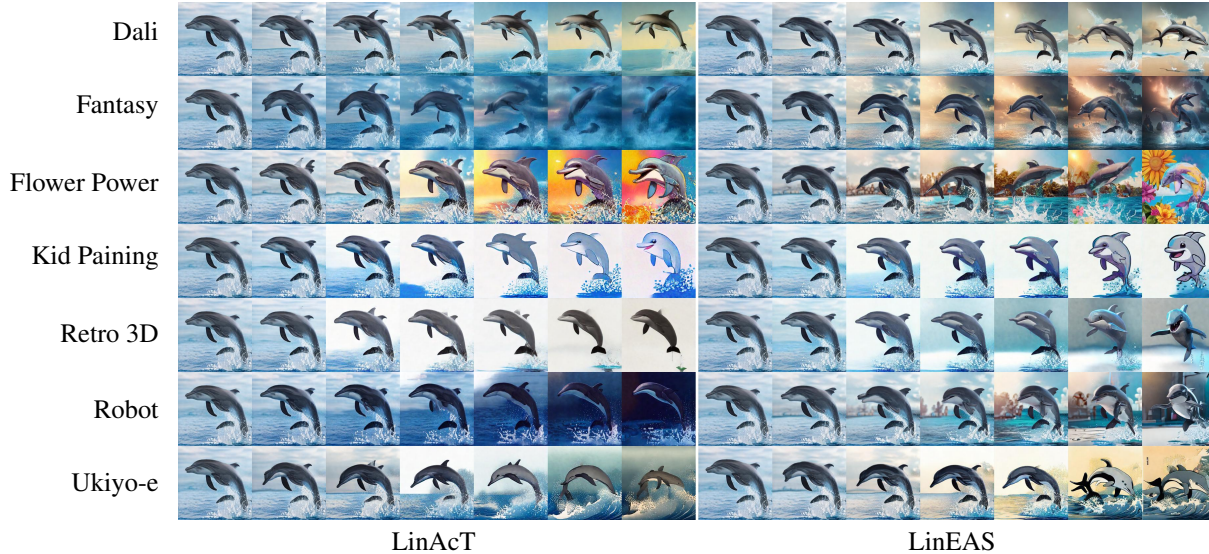


Figure 11. Images generated for the prompt *A playful dolphin jumping out of water*. The left panel contains images generated with Lin-ACT and the right panel with LinEAS. Each row contains images generated with a different style and each column corresponds to a different strength $\lambda \in [0, 0.15, 0.30, 0.45, 0.60, 0.85, 1.0]$.

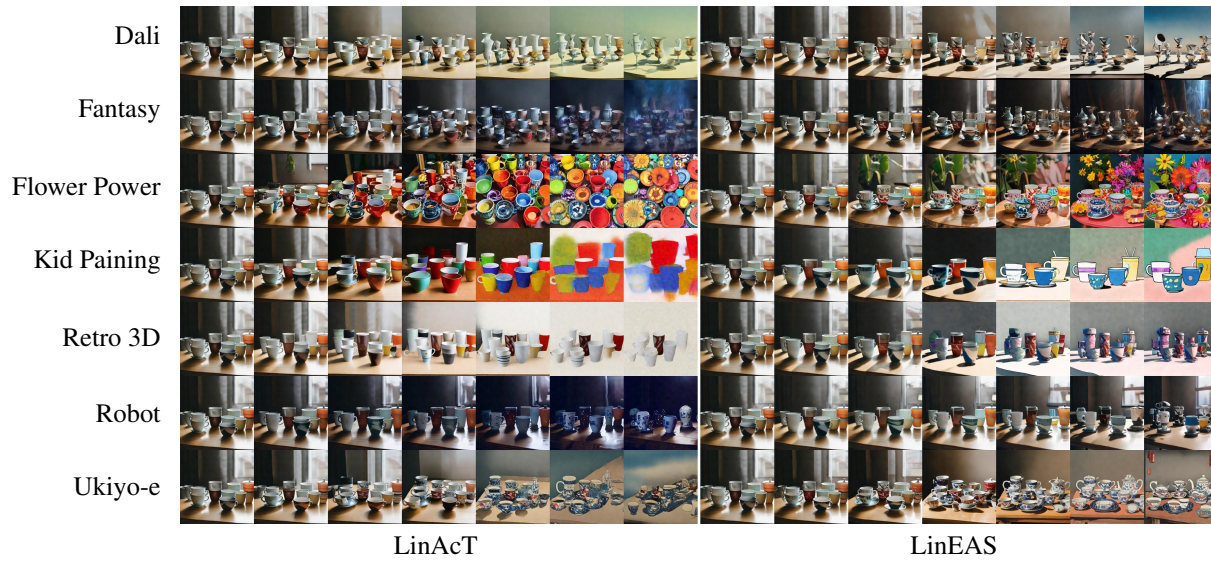


Figure 12. Images generated for the prompt *Various cups on a table..*. The left panel contains images generated with Lin-ACT and the right panel with LinEAS. Each row contains images generated with a different style and each column corresponds to a different strength $\lambda \in [0, 0.15, 0.30, 0.45, 0.60, 0.85, 1.0]$.

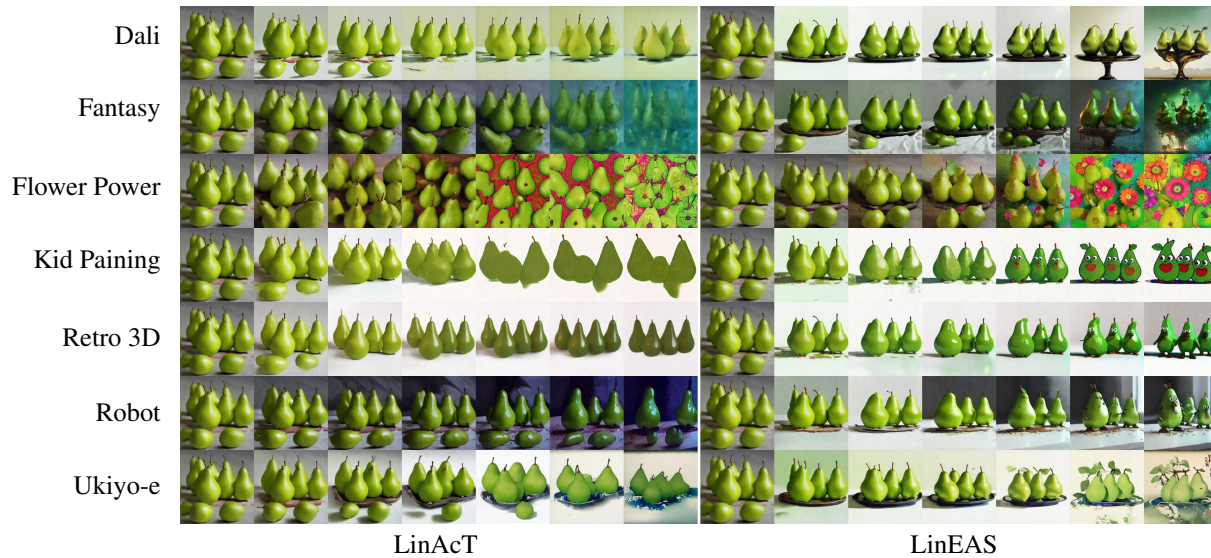


Figure 13. Images generated for the prompt *Green pears arranged artistically.*. The left panel contains images generated with Lin-ACT and the right panel with LinEAS. Each row contains images generated with a different style and each column corresponds to a different strength $\lambda \in [0, 0.15, 0.30, 0.45, 0.60, 0.85, 1.0]$.

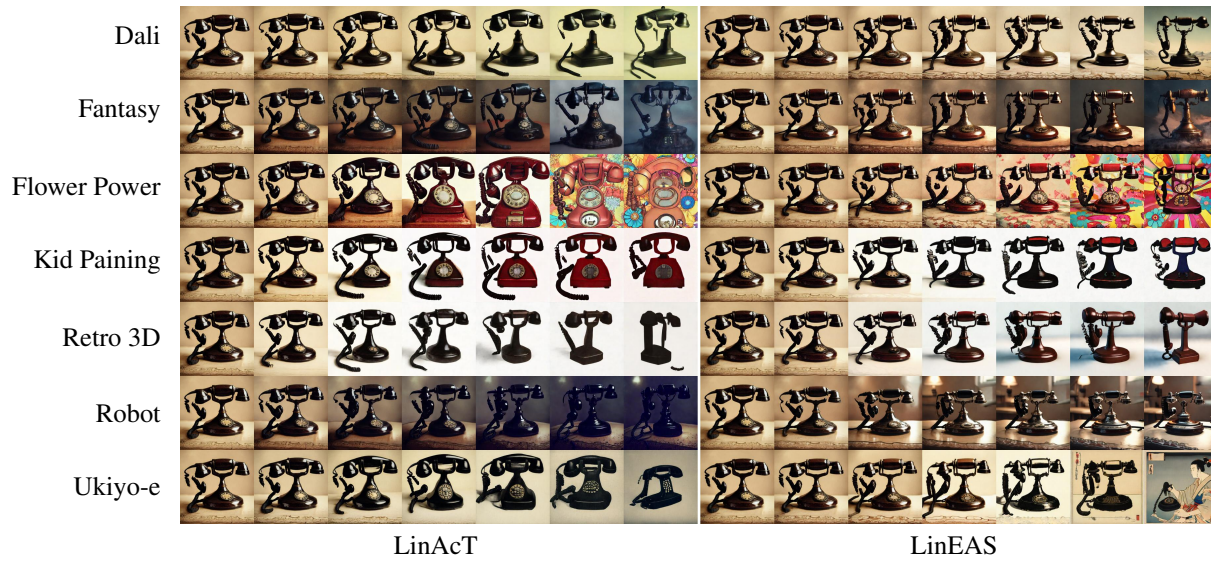


Figure 14. Images generated for the prompt *An old-style telephone receiver.* The left panel contains images generated with Lin-ACt and the right panel with LinEAS. Each row contains images generated with a different style and each column corresponds to a different strength $\lambda \in [0, 0.15, 0.30, 0.45, 0.60, 0.85, 1.0]$.

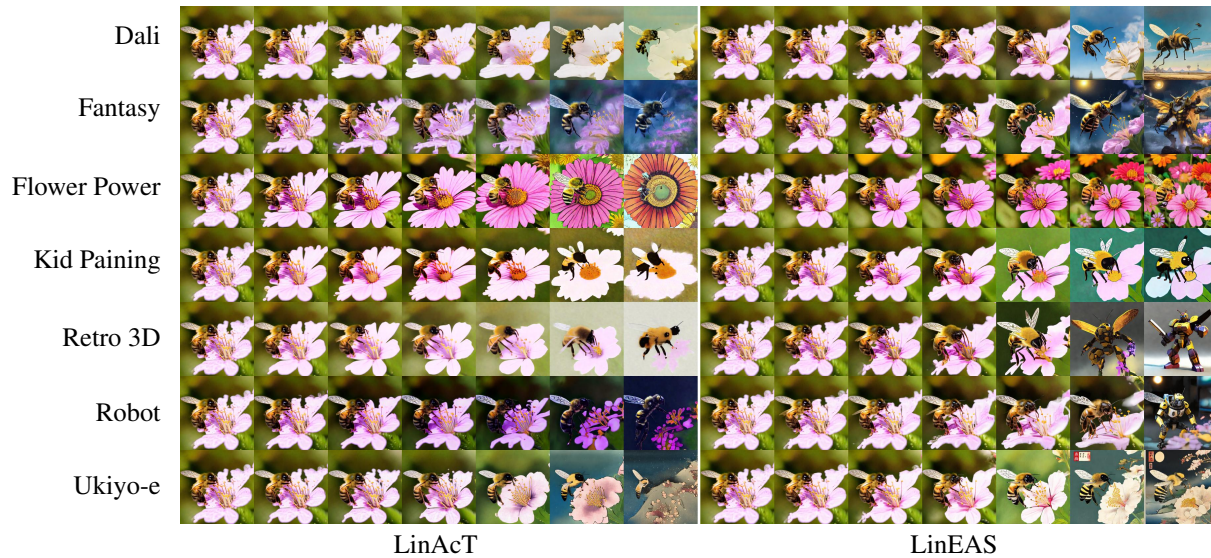


Figure 15. Images generated for the prompt *A busy bee collecting nectar.* The left panel contains images generated with Lin-ACt and the right panel with LinEAS. Each row contains images generated with a different style and each column corresponds to a different strength $\lambda \in [0, 0.15, 0.30, 0.45, 0.60, 0.85, 1.0]$.

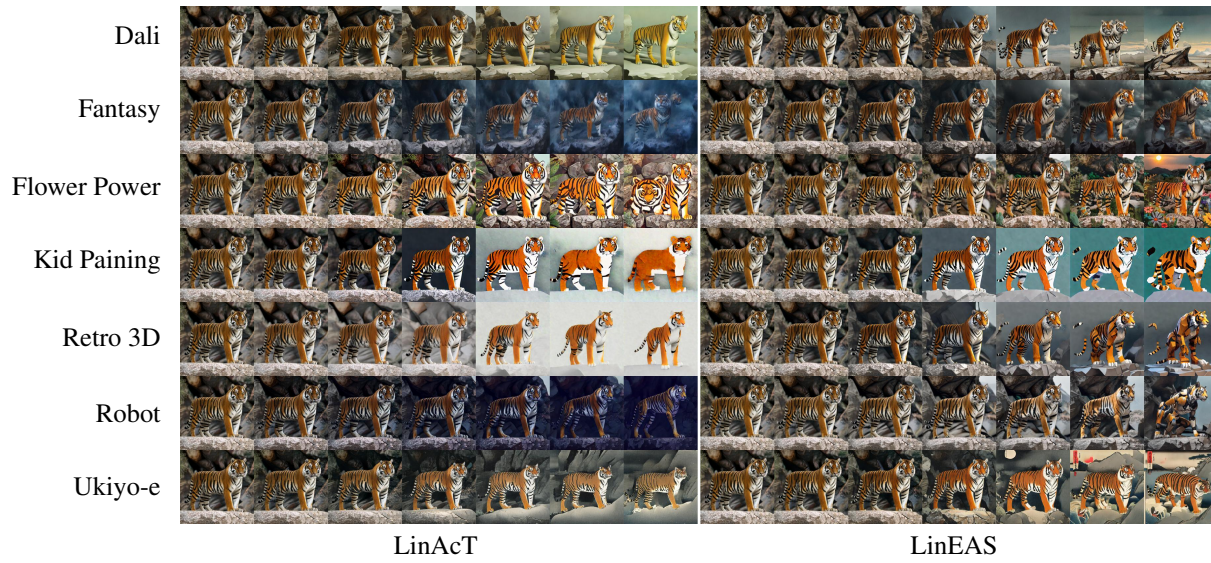


Figure 16. Images generated for the prompt *A tiger standing on rocky terrain*. The left panel contains images generated with Lin-ACt and the right panel with LinEAS. Each row contains images generated with a different style and each column corresponds to a different strength $\lambda \in [0, 0.15, 0.30, 0.45, 0.60, 0.85, 1.0]$.

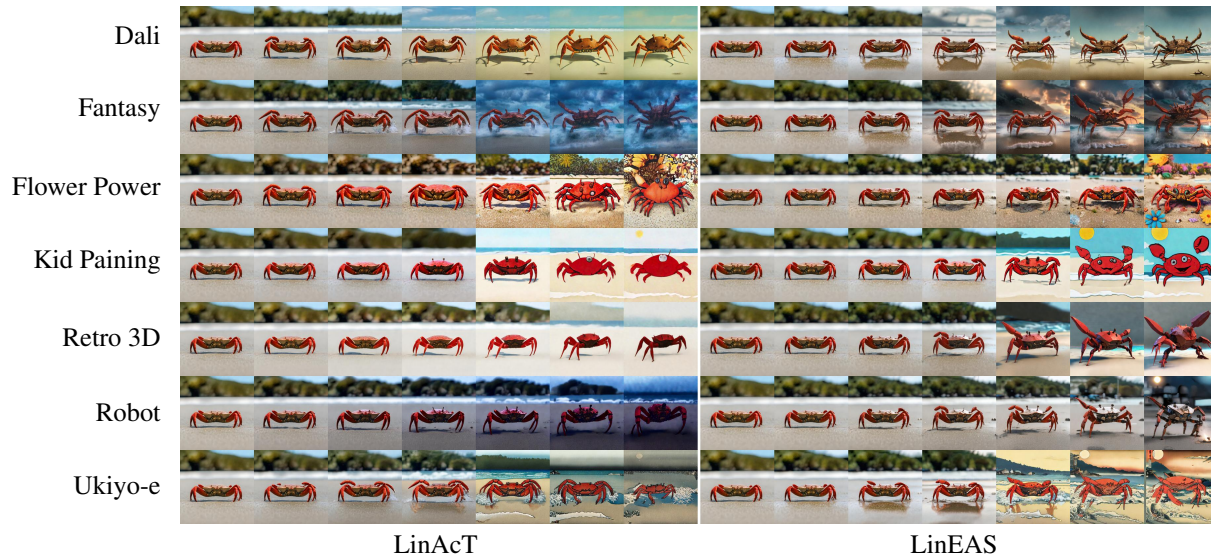


Figure 17. Images generated for the prompt *A crab scuttling across the beach*. The left panel contains images generated with Lin-ACt and the right panel with LinEAS. Each row contains images generated with a different style and each column corresponds to a different strength $\lambda \in [0, 0.15, 0.30, 0.45, 0.60, 0.85, 1.0]$.

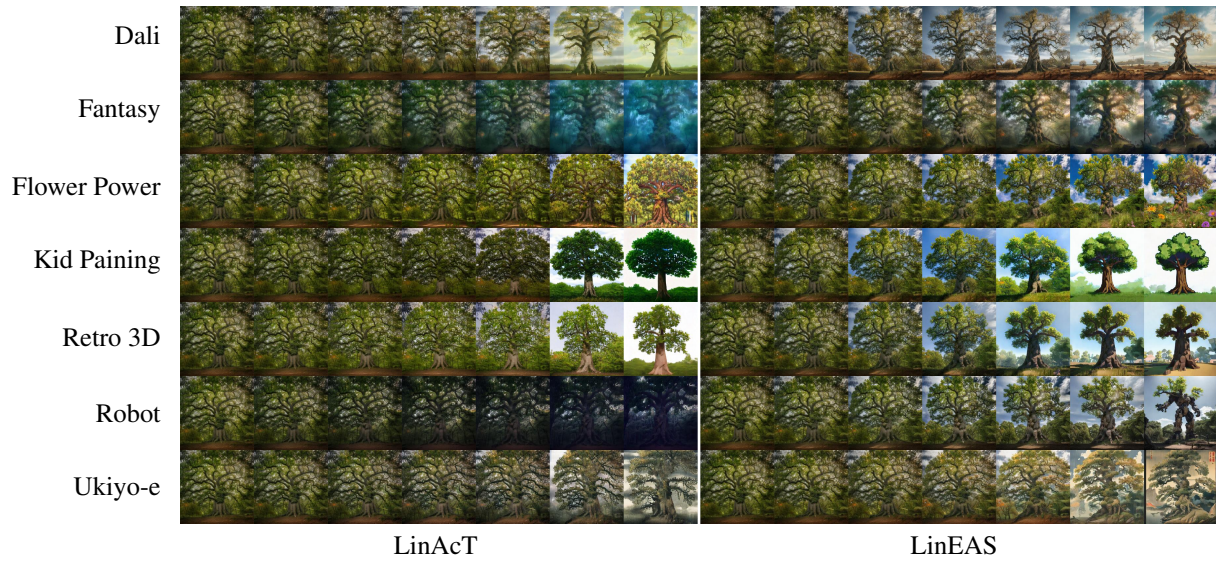


Figure 18. Images generated for the prompt *An oak tree standing tall in the forest*. The left panel contains images generated with Lin-ACT and the right panel with LinEAS. Each row contains images generated with a different style and each column corresponds to a different strength $\lambda \in [0, 0.15, 0.30, 0.45, 0.60, 0.85, 1.0]$.

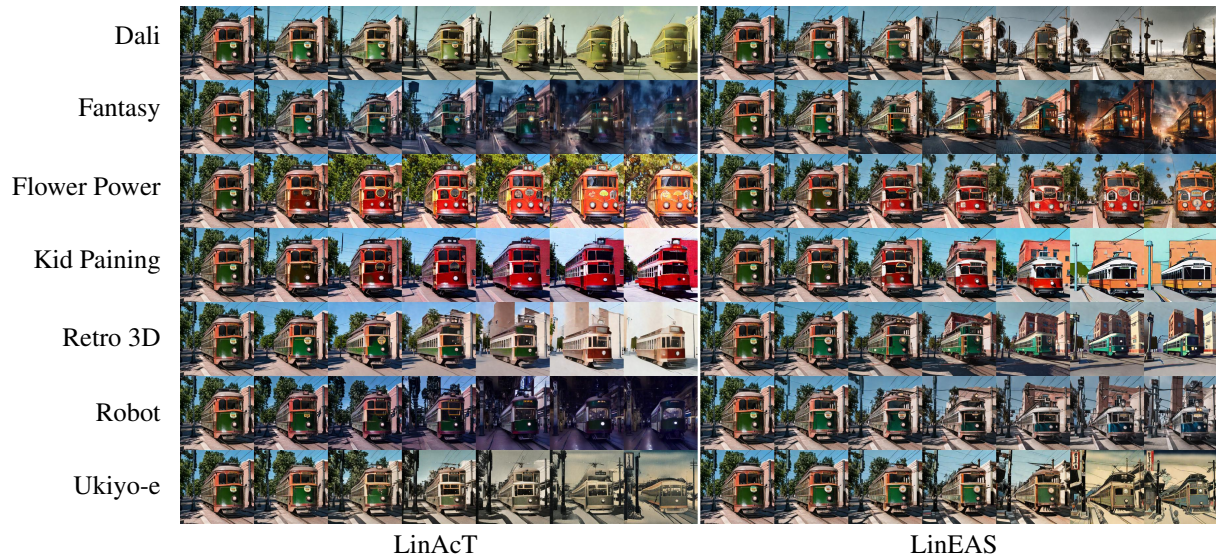


Figure 19. Images generated for the prompt *An old streetcar pulling into a station*. The left panel contains images generated with Lin-ACT and the right panel with LinEAS. Each row contains images generated with a different style and each column corresponds to a different strength $\lambda \in [0, 0.15, 0.30, 0.45, 0.60, 0.85, 1.0]$.

I. Diffusion prompts

We train LinEAS to transport activations from a source distribution (p) of 32 unconditional prompts to a conditional one (q) of 32 prompts.

For style transfer, we follow [Rodriguez et al. \(2025\)](#) and sample p from the COCO Captions dataset ([Chen et al., 2015](#)). The target distribution q is also obtained from COCO Captions by appending different tags that induce styles in the generated images (*e.g.* art nouveau). We refer the reader to [Rodriguez et al. \(2025\)](#) for the exact list of such tags.

To induce concepts, we prompt a large language model to generate a diverse set of 32 prompts that describe a certain concept. We provide a sample of the prompts we used in [Table 8](#) and the full set of prompts is provided as supplementary material.

Source	<p>A beaver in its natural habitat.</p> <p>Poppies swaying gently in a field.</p> <p>A train passing through mountains.</p> <p>A sturdy table with drawers.</p>
Flower Power	<p>Vibrant hippie flower-power blooms in a peaceful meadow, surrounded by butterflies. #flowerpower #hippievibes</p> <p>Psychedelic flower-power design with bold patterns, peace signs, and groovy colors. #flowerpower #hippietide</p> <p>Hippie van with flower decals in a field of daisies under a colorful sky. #flowerpower #groovyhippie</p> <p>Flower crowns and peace signs on hippie people in a grassy field. #hippievibes #flowerpower</p>
Robots	<p>A sleek silver robot waves hello in a futuristic city.</p> <p>A tiny robot with glowing eyes explores a dark cave.</p> <p>A giant battle robot towers over a ruined metropolis.</p> <p>A robot chef flips pancakes in a high-tech kitchen.</p>
Fantasy	<p>A majestic dragon flying over a glowing crystal mountain range, under a purple sky, fantasy art</p> <p>A knight in shining armor standing before a towering, ancient forest, mist swirling around, high fantasy</p> <p>A wizard casting a spell by a crystal-clear lake, surrounded by ethereal lights, magical realism</p> <p>Elven warriors riding glowing horses through a mystical forest, high fantasy</p>
Salvador Dali	<p>A melting clock draped over a desert cactus, with elongated shadows – surrealism, Dali style.</p> <p>A distorted landscape with floating spheres and twisted trees – Salvador Dali inspired, dreamlike.</p> <p>A desert horizon with a distorted figure of a horse, shadow stretching into infinity – Dali-esque.</p> <p>A distorted face morphing into a tree, set in an eerie landscape – Salvador Dali inspired.</p>
Retro 3D graphics	<p>3D polygon character with blocky features, low-resolution textures, visible aliasing, retro video-console graphics style</p> <p>Video-Console environment with pixelated textures, jagged edges, and low-poly models</p> <p>3D car with jagged polygons, low-resolution reflections, console graphics aesthetic</p> <p>Polygonal character in a simplistic 3D world with aliasing and low-quality textures</p>
Kid’s Paintings	<p>A cartoon sun with a face, big yellow rays, and a blue sky, Paint style #childish #simple #hand-drawn</p> <p>A red house with a triangle roof, green windows, and a blue door, drawn in MS Paint #kidsart #colorful #blocky</p> <p>A smiling green dinosaur with orange spikes, drawn like a child in Paint #childlike #simple #brightcolors</p> <p>A purple cat with big eyes, sitting on a pink carpet, Paint style #cute #blocky #basicshapes</p>
Ukiyo-e	<p>A majestic view of Mount Fuji, cherry blossoms in full bloom, woodblock print style, Ukiyo-e, Edo period aesthetics</p> <p>A stormy sea with giant waves crashing, a lone boat struggling against the current, traditional Japanese woodblock print, Ukiyo-e</p> <p>A peaceful Zen garden covered in autumn leaves, intricate textures, Ukiyo-e, traditional ink and woodblock style</p> <p>A winding river through a dense bamboo forest, soft mist rising, stylized clouds, Ukiyo-e, Edo period style</p>

Table 8. Sample prompts used to induce concepts in text to image generation.